

Article

Gadolinium Doping Modulates the Enzyme-like Activity and Radical-Scavenging Properties of CeO₂ Nanoparticles

Madina M. Sozarukova ¹, Taisiya O. Kozlova ¹, Tatiana S. Beshkareva ^{1,2}, Anton L. Popov ³, Danil D. Kolmanovich ³, Darya A. Vinnik ³, Olga S. Ivanova ⁴, Alexey V. Lukashin ², Alexander E. Baranchikov ¹ and Vladimir K. Ivanov ^{1,*}

¹ Kurnakov Institute of General and Inorganic Chemistry of the Russian Academy of Sciences, 119991 Moscow, Russia

² Materials Science Department, Lomonosov Moscow State University, 119234 Moscow, Russia

³ Institute of Theoretical and Experimental Biophysics of the Russian Academy of Sciences, 142290 Pushchino, Russia

⁴ Frumkin Institute of Physical Chemistry and Electrochemistry of the Russian Academy of Sciences, 119071 Moscow, Russia

* Correspondence: van@igic.ras.ru

Abstract: Their unique physicochemical properties and multi-enzymatic activity make CeO₂ nanoparticles (CeO₂ NPs) the most promising active component of the next generation of theranostic drugs. When doped with gadolinium ions, CeO₂ NPs constitute a new type of contrast agent for magnetic resonance imaging, possessing improved biocatalytic properties and a high level of biocompatibility. The present study is focused on an in-depth analysis of the enzyme-like properties of gadolinium-doped CeO₂ NPs (CeO₂:Gd NPs) and their antioxidant activity against superoxide anion radicals, hydrogen peroxide, and alkylperoxyl radicals. Using an anion-exchange method, CeO₂:Gd NPs (~5 nm) with various Gd-doping levels (10 mol.% or 20 mol.%) were synthesized. The radical-scavenging properties and biomimetic activities (namely SOD- and peroxidase-like activities) of CeO₂:Gd NPs were assessed using a chemiluminescent method with selective chemical probes: luminol, lucigenin, and L-012 (a highly sensitive luminol analogue). In particular, gadolinium doping has been shown to enhance the radical-scavenging properties of CeO₂ NPs. Unexpectedly, both bare CeO₂ NPs and CeO₂:Gd NPs did not exhibit SOD-like activity, acting as pro-oxidants and contributing to the generation of reactive oxygen species. Gadolinium doping caused an increase in the pro-oxidant properties of nanoscale CeO₂. At the same time, CeO₂:Gd NPs did not significantly inhibit the intrinsic activity of the natural enzyme superoxide dismutase, and CeO₂:Gd NPs conjugated with SOD demonstrated SOD-like activity. In contrast to SOD-like properties, peroxidase-like activity was observed for both bare CeO₂ NPs and CeO₂:Gd NPs. This type of enzyme-like activity was found to be pH-dependent. In a neutral medium (pH = 7.4), nanoscale CeO₂ acted as a prooxidant enzyme (peroxidase), while in an alkaline medium (pH = 8.6), it lost its catalytic properties; thus, it cannot be regarded as a nanozyme. Both gadolinium doping and conjugation with a natural enzyme were shown to modulate the interaction of CeO₂ NPs with the key components of redox homeostasis.

Keywords: nanozyme; nanoceria; gadolinium; conjugate; antioxidant; prooxidant; radical scavenger; chemiluminescence



Citation: Sozarukova, M.M.; Kozlova, T.O.; Beshkareva, T.S.; Popov, A.L.; Kolmanovich, D.D.; Vinnik, D.A.; Ivanova, O.S.; Lukashin, A.V.; Baranchikov, A.E.; Ivanov, V.K. Gadolinium Doping Modulates the Enzyme-like Activity and Radical-Scavenging Properties of CeO₂ Nanoparticles. *Nanomaterials* **2024**, *14*, 769. <https://doi.org/10.3390/nano14090769>

Academic Editor: Constantine D. Stalikas

Received: 22 March 2024

Revised: 17 April 2024

Accepted: 24 April 2024

Published: 26 April 2024



Copyright: © 2024 by the authors. Licensee MDPI, Basel, Switzerland. This article is an open access article distributed under the terms and conditions of the Creative Commons Attribution (CC BY) license (<https://creativecommons.org/licenses/by/4.0/>).

1. Introduction

Today, there is an urgent need for the development of theranostic agents combining both diagnostic and therapeutic properties, as well as advanced antioxidants capable of scavenging different types of free radicals [1–3]. This is especially true in the context of the treatment of complex diseases with heterogeneous expressions such as malignant tumors, where the use of standard clinical approaches for their diagnosis and treatment may be ineffective [4–6]. Metal oxide nanoparticles demonstrate impressive biological activity and

are considered to be promising components for the creation of multifunctional theranostic agents [7–9]. These inorganic nanobiomaterials are characterized by a number of important physicochemical properties, such as ultrasmall particle size, high reactivity, biocompatibility and immunogenicity, which make them suitable for biomedical applications [4,10].

CeO₂ nanoparticles (CeO₂ NPs), which represent a new class of inorganic nanobiomaterial with enzyme-like activity (nanozymes), attract special attention. The increased interest of researchers in nanoscale CeO₂ is due to its ability to self-regenerate and its multi-enzymatic activity [11–13]. CeO₂ nanoparticles demonstrate superoxide dismutase- (SOD-) [14–17], catalase- [18–20], peroxidase- [21,22], oxidase- [23,24], phosphatase- [25], photolyase- [26], phospholipase- [27], nuclease- [28], haloperoxidase- [29], lipo-/phospholipoperoxidase- [30] and uricase-like [31] activities. The multi-enzymatic activity of nanoscale CeO₂ is known to be strongly pH-dependent [23,32]. This enables switching between the anti- and prooxidant properties of CeO₂ NPs, which is extremely important for biomedical applications.

The biological activity of CeO₂ NPs can be affected by various factors [33,34], one of which is the surface oxidation state, which is believed to significantly affect the enzyme-mimetic activities of nanoscale CeO₂ [35]. Numerous methods and approaches have been described for regulating the surface structure of inorganic nanomaterials [33,36]. Doping CeO₂ NPs with the ions of transition and rare earth elements (REEs) is an approach of choice for obtaining multifunctional nanozymes based on nanoscale CeO₂ for practical applications [33,37]. According to a widespread assumption, doping CeO₂ NPs with REE ions (Eu, Er, Nd, Pr, La, Sm) leads to an increase in the concentration of oxygen vacancies and an increase in the Ce³⁺/Ce⁴⁺ ion ratio on the surface [38,39]. At the same time, there are controversial data in the literature on the effect of doping ceria with REE ions on its biological activity and catalytic characteristics while maintaining high oxygen non-stoichiometry [38–41].

Doping CeO₂ NPs with Gd ions to obtain a new class of contrast agents for magnetic resonance imaging is of particular interest for the development of advanced hybrid theranostic agents [4,42]. Prospects for the creation of such hybrid nanobiomaterials based on nanoscale CeO₂ are subject to the following considerations. On the one hand, the content of surface Ce³⁺ ions and the biocatalytic properties of CeO₂ NPs can be further enhanced by modification with gadolinium ions [4,43]. On the other hand, there is an issue with using Gd-based complexes as contrast agents, due to the high toxicity associated with free gadolinium ions (those ions that are not incorporated into a crystal structure or part of a complex) [44,45]. In this regard, strategies to reduce the dosage of Gd are being actively developed to improve contrasting ability (relaxivity). To achieve this, nanoparticles containing Gd are produced [46,47] that are stabilized with biocompatible ligands [48,49] and conjugated with targeting biomolecules [50,51].

It should be noted that most studies have focused on the features of the surface state of CeO₂ NPs when doped with Gd, and on some aspects of the biological activity of this type of material. At the same time, there remains a need for a comprehensive analysis of the multi-functional biomimetic activities of ceria-based nanozymes, especially those doped with gadolinium and other rare earth elements.

To date, some progress has been achieved in this direction. Composites based on gadolinium-doped CeO₂ NPs (CeO₂:Gd NPs) have been reported as being multifunctional agents for magnetic resonance imaging and computed tomography [38,39,52]. These composites have demonstrated improved sensitivity for tumor detection [38] and high T₁ relaxivity [52], good biocompatibility [52] and stability in biological milieu [38]; they have also exhibited high enzyme-like activity [39] and selective cytotoxicity to cancer cells [52].

The current study is focused on a comparative analysis of the biomimetic activity and radical-scavenging properties (antioxidant activity) of CeO₂:Gd NPs. The biochemical behavior of CeO₂:Gd NPs was investigated in relation to the key components of redox homeostasis—superoxide anion radicals, hydrogen peroxide, and alkylperoxyl radicals. The biomimetic activities, namely SOD- and peroxidase-like activities, and radical-

scavenging properties of CeO₂:Gd NPs were assessed using a chemiluminescent method with selective probes: lucigenin, 8-amino-5-chloro-7-phenyl-pyrido [3,4-d]pyridazine-1,4(2H,3H)dione, and luminol, respectively. Both bare CeO₂ NPs and CeO₂:Gd NPs synthesized using an ion-exchange method followed by hydrothermal treatment demonstrated pronounced peroxidase-like biomimetic activity and radical-scavenging properties. Unexpectedly, bare CeO₂ NPs and CeO₂:Gd NPs showed no SOD-mimetic activity while not significantly inhibiting the activity of the natural superoxide dismutase enzyme in the NP-SOD conjugates. The results obtained may be of fundamental importance for understanding the features and mechanisms of the modulation of the nanozyme activity of CeO₂ NPs by gadolinium doping and conjugation with SOD.

2. Materials and Methods

2.1. Materials (Chemicals)

The following reagents were used in this work: Ce(NO₃)₃·6H₂O (LANHIT, Moscow, Russia, 99.9%), Gd(NO₃)₃·6H₂O (Sigma Aldrich, St. Louis, MO, USA, 99.9%), NH₄OH (Chimmed, Moscow, Russia, puriss. spec.), Amberlite IRA-410 anion exchange resin (Sigma Aldrich), NaOH (Sigma Aldrich, ≥98%), hydrochloric acid (SigmaTech, Arlington, VA, USA, puriss. spec.), ammonium citrate dibasic (Sigma Aldrich, ≥98%), isopropyl alcohol (Chimmed, puriss. spec.).

2.2. Methods for the Synthesis of Aqueous Sols of Cerium Dioxide, Including Those Doped with Gadolinium

The synthesis of aqueous cerium dioxide sols and ceria-gadolinia solid solutions was carried out in accordance with a previously described method [53]. First, the anion exchange resin (Cl form) was converted to the OH form. For this, the anion exchange resin was soaked in a 10% NaOH solution and stirred for one day, after which the supernatant liquid was removed and the resin was soaked in a new portion of the NaOH solution. This procedure was carried out for one week. Next, the resin was repeatedly washed with distilled water.

Anion exchange resin was gradually added to 100 mL of a 0.01 M solution of Ce(NO₃)₃·6H₂O (0.434 g), with stirring, to pH = 9.6. Then, the resin was separated by decantation. Next, the solution, in a Teflon autoclave, was incubated in a drying oven for 12 h at 190 °C.

The method for preparing aqueous sols of solid solutions of cerium dioxide doped with gadolinium was similar to the method for synthesizing aqueous sols of bare cerium dioxide. At the initial stage, a mixed solution of Ce(NO₃)₃·6H₂O and Gd(NO₃)₃·6H₂O was prepared at such concentrations that the molar content of gadolinium in the final product was 10% or 20%.

As a control in chemiluminescence measurements, a solution was used that was obtained by preparing a suspension of anion exchange resin (OH form) with pH 9.6, decanting the resin, and then subjecting the mother solution to hydrothermal treatment at 190 °C for 12 h.

2.3. Materials Characterisation

Powder X-ray diffraction analysis (XRD) of the samples was carried out on a Bruker D8 Advance diffractometer, Bruker, Billerica, MA, USA (CuKα radiation, θ–2θ geometry) in the angle range of 3–120° 2θ, with a step of 0.01–0.02° 2θ and a signal accumulation time of at least 0.3 s per point. JANA2006 software was used for full-profile analysis of diffraction patterns. The crystallite sizes were assessed using the Scherrer equation $D = \frac{180K\lambda}{\pi L_x}$, where D is the crystallite size, K is the Scherrer constant, λ is the X-ray wavelength, and L_x is the full-profile analysis parameter in JANA2006 software.

The determination of the atomic ratio of cerium and gadolinium in the solid state products obtained was carried out by Energy-dispersive X-ray spectroscopy (EDX) on an NVision 40 microscope (Carl Zeiss, Jena, Germany), using an X-MAX 80 mm² energy-dispersive detector. The analysis was carried out at an accelerating voltage of 20 kV. The

elemental composition was calculated in a semi-automatic mode, using INCA Oxford software (Oxford Instruments, Oxford, UK, version 2.1).

The microstructure of the samples was studied by transmission electron microscopy (TEM), using a Leo912 AB Omega electron microscope (Carl Zeiss, Jena, Germany) at an accelerating voltage of 100 kV. The samples were placed on copper grids with a diameter of 3.05 mm, coated with a polymer film. Transmission images were obtained at magnifications up to $\times 500,000$.

UV-vis absorption spectra of CeO₂ sols were recorded using a UV-vis-NIR spectrophotometer (Cary 5000, Agilent, Santa Clara, CA, USA) at room temperature. The absorption spectrum of distilled water was used as the baseline.

The particle size distribution was obtained using a Photocor Complex multi-angle dynamic light scattering spectrometer with a diode laser ($\lambda = 650$ nm, radiation power 25 mW). All measurements were carried out at a scattering angle of 90°.

Raman spectra were recorded on a Renishaw InVia Reflex spectrometer (Renishaw, Dundee IL, USA) using a Renishaw 633 nm HeNe laser (radiation power 3 mV); spectrum accumulation time was 100 s and data were averaged over three spectra.

2.4. Preparation of Ceria-SOD Conjugates

A stock solution of Cu,Zn-superoxide dismutase (SOD, #S8160-15KU, Sigma, Kawasaki-shi, Japan) with an activity of 2400 U/mL ($c = 25$ μ M) was prepared by quickly dissolving a sample of SOD in deionized water (18 MOhm cm). Conjugates of CeO₂ NPs and CeO₂:Gd NPs with SOD were prepared according to a previously described procedure [54]. Briefly, an aqueous solution of SOD with an activity of 100 U/mL ($c = 1$ μ M) was mixed with 10 mM CeO₂ sol or 10 mM CeO₂:Gd sol. The mixtures were incubated for 60 min in the dark at room temperature.

2.5. Analysis of Enzyme-like Activity and Radical-Scavenging Properties

As a blank in chemiluminescent measurements, a reaction mixture without the analyzed sample was used. The blank includes a phosphate buffer solution, a radical initiator and a chemiluminescent probe.

2.5.1. SOD-Mimetic Assay

To analyze the SOD-like activity of ceria sols, a chemiluminescence method was used, based on recording the chemiluminescence of lucigenin during its oxidation by superoxide anion radicals ($\bullet\text{O}_2^-$). The generation of superoxide anion radicals occurs as a result of the oxidation of xanthine to uric acid in the presence of oxygen [55,56].

Aliquots of aqueous solutions of xanthine (20 μ M, #X0626, Sigma), lucigenin (20 μ M, #393824, J&K, San Jose, CA, USA), and the test sample were rapidly added to a cuvette with a phosphate buffer solution (100 mM, pH = 7.4). The background signal was recorded for 30–60 s, and then xanthine oxidase ($a = 8.8$ mU/mL, #X1875-25UN, Sigma) was added. The intensity of chemiluminescence was recorded at 37 °C on a 12-channel Lum-1200 chemiluminometer (DISoft, Moscow, Russia). All experiments were conducted in triplicate. The results were processed using PowerGraph software (version 3.3).

2.5.2. Peroxidase Mimetic Assay

The peroxidase-like activity of ceria sols was analyzed with respect to hydrogen peroxide in the presence of L-012 (8-amino-5-chloro-7-phenyl-pyrido [3,4-d]pyridazine-1,4(2H,3H)dione), which is a highly sensitive luminol analogue [57,58].

Aliquots of H₂O₂ (20 μ M, #H1009, Sigma) and L-012 (10 μ M, #SML2236, Sigma) were rapidly added to a cuvette with a phosphate buffer solution (100 mM, pH = 7.4). The background signal was recorded for 60–90 s. An aliquot of the test sample was added after the chemiluminescence intensity reached a stationary value. All experiments were conducted in triplicate. Chemiluminescence was recorded on a 12-channel Lum-

1200 chemiluminometer (DISoft, Russia). The results were processed using PowerGraph software (version 3.3).

The chemiluminescence curves were used for kinetic modeling and estimating the kinetic constants for the interaction of ceria nanoparticles with the substrate. Mathematical modeling of chemiluminograms was carried out using the Kinetic Analyzer software (<http://www.powergraph.ru/soft/>) [55,59].

2.5.3. Analysis of Radical-Scavenging Properties

To analyze the radical scavenging properties of ceria sols, a model reaction of the generation of alkylperoxyl radicals ($\text{ROO}\bullet$) during the decomposition of 2,2'-azobis(2-amidinopropane) dihydrochloride (AAPH) was used [60].

AAPH (2.5 μM , #123072, Sigma) and luminol (2.0 μM , #123072, Sigma) were rapidly added to a cuvette thermostated at 37 °C with a phosphate buffer solution (100 mM, pH = 7.4). An aliquot of the test sample was added after the chemiluminescence intensity reached a stationary value. Chemiluminescence was recorded on a 12-channel Lum-1200 chemiluminometer (DISoft, Russia).

2.5.4. Statistical Analysis

All experiments were conducted in triplicate. The experimental results of enzyme-like and radical-scavenging activities were processed using PowerGraph software (version 3.3). Cytotoxicity analysis and cell culture experiments were processed using GraphPad Prism 8 software (version 8.0). The MTT assay data are presented as $M \pm SD$. The statistical significance of the deviations between the test sets and the control was confirmed using the Mann-Whitney U test. Images were processed using Adobe Photoshop CC software 2017.

3. Results and Discussion

3.1. Characterisation of CeO_2 NPs and Gadolinium-Doped CeO_2 NPs

Three transparent solutions were obtained through anion exchange treatment of aqueous solutions of cerium and gadolinium (0%, 10%, 20%) nitrates followed by hydrothermal synthesis, in which a distinct Tyndall cone was observed. The concentration of sols was 0.01 M, as determined by the thermogravimetric method. Figure 1 shows the UV-vis absorption spectra of CeO_2 sols with different levels of Gd doping.

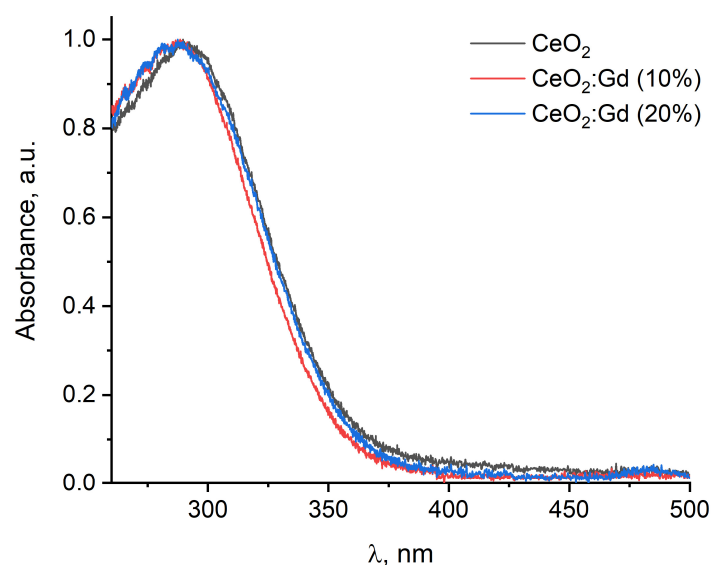


Figure 1. Electron absorption spectra of cerium dioxide sols with different levels of gadolinium doping.

The UV-vis spectra of both the bare CeO_2 NPs and $\text{CeO}_2:\text{Gd}$ NPs are typical of nanocrystalline cerium dioxide and contain a broad absorption band with a maximum

in the region of 290–300 nm (Figure 1). The determined band gap values for all samples were nearly 3.4 and 3.8 eV for indirect and direct transitions, respectively, which agree with previously reported data [53,61].

According to dynamic light scattering data, the hydrodynamic radii of the particles in ceria sols were generally close to one another, measuring about 10–15 nm.

Ceria sols dried at 60 °C were analyzed by XRD. As revealed by the XRD patterns, the samples of bare CeO₂ NPs and CeO₂:Gd NPs (Figure 2a) were single-phase cerium dioxide with a fluorite structure (PDF2 No. 34-394), which is in good agreement with the literature [33,62,63]. At gadolinium concentrations of up to 20%, no gadolinium-containing impurity phases were detected in the obtained samples, which indirectly confirms the inclusion of Gd cations in the CeO₂ structure.

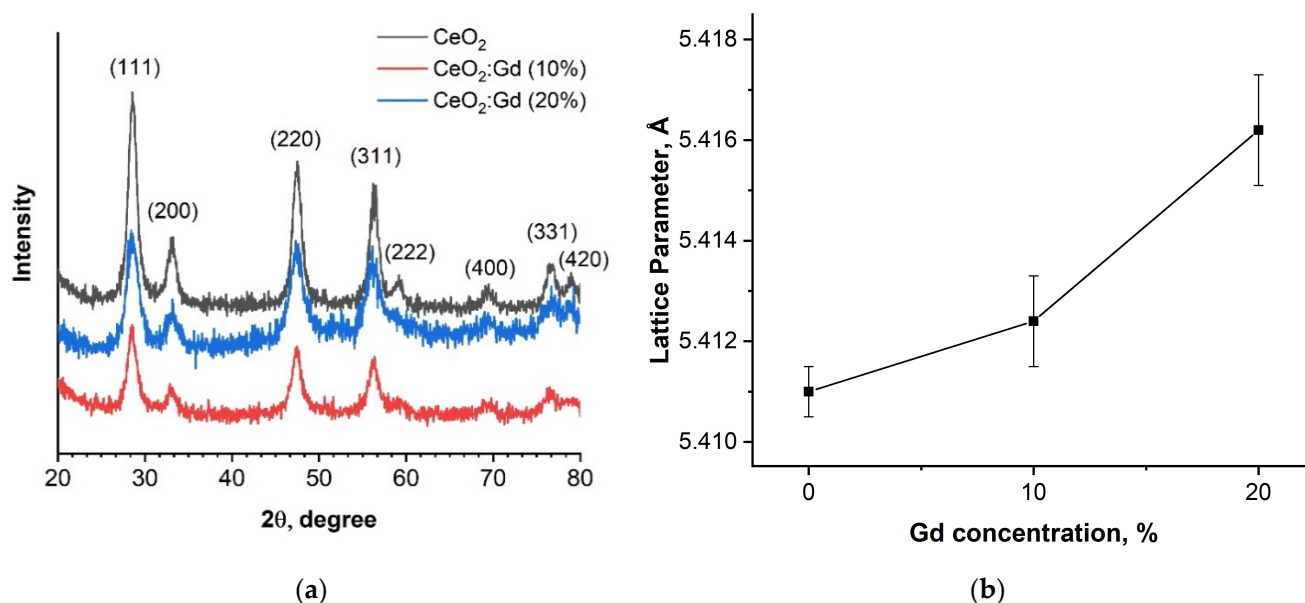


Figure 2. (a) Diffractograms of CeO₂ samples with different levels of Gd doping; (b) dependence of the unit cell parameters on the nominal gadolinium content.

Diffraction maxima at 28.5°, 33.0°, 47.5°, 56.4°, 59.1°, 69.4°, 76.6°, and 79.1° correspond to (111), (200), (220), (311), (222), (400), (331), and (420) CeO₂ crystallographic planes, respectively (Figure 2a) [33,64]. The unit cell parameters calculated using a full profile analysis of diffraction patterns are presented in Figure 2b. The unit cell parameter increased almost linearly, which was caused by the incorporation of a Gd³⁺ ion in the CeO₂ structure, since the ionic radius of Gd³⁺ (0.107 nm) is larger than the ionic radius of Ce⁴⁺ (0.097 nm) [29,33,37,62,65].

According to EDX data, the average Ce:Gd ratio in gadolinium-doped ceria samples was 89.6:10.4 and 77.9:22.1, which is very close to the nominal gadolinium content (10% and 20%). This further confirms the successful synthesis of solid solutions of CeO₂:Gd (10%, 20%) by the ion-exchange method followed by hydrothermal treatment.

Figure 3 shows the Raman spectra of bare CeO₂ NPs and CeO₂:Gd NPs.

The spectra of all the samples show a characteristic Raman peak at 464 cm⁻¹, corresponding to symmetric vibrations of oxygen ions in CeO₈ octahedra [33,66,67]. For CeO₂:Gd NPs, a shift of the Raman peaks to lower energies and their broadening can be observed, in comparison with bare CeO₂ NPs, which can be explained by an increase in the unit cell parameter, including that caused by doping [66,68,69]. At a 20% doping level, peaks at 550 cm⁻¹ and 605 cm⁻¹ appear in the Raman spectrum. This reflects an increase in the concentration of oxygen vacancies and provides further evidence for the formation of solid solutions [66,70].

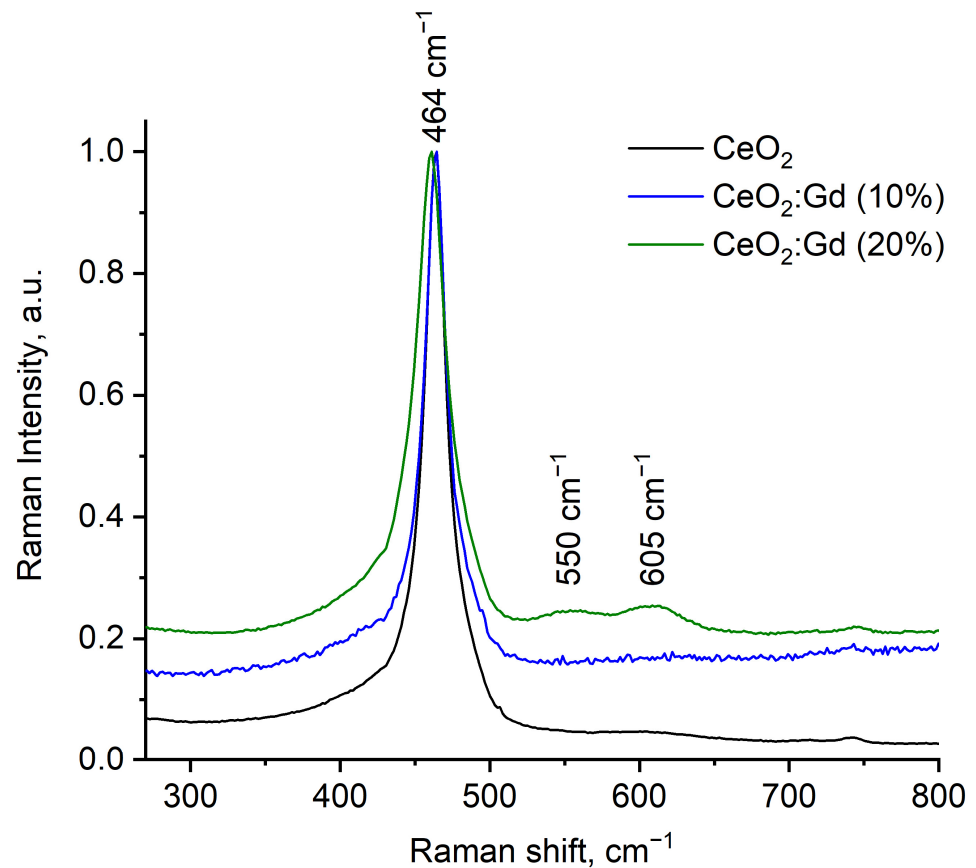


Figure 3. Raman spectra of dried aqueous cerium dioxide sols with different levels of gadolinium doping.

TEM and electron diffraction data (Figure 4) indicate that the introduction of gadolinium had little effect on the shape and size of CeO_2 particles (Figure 5). CeO_2 and $\text{CeO}_2:\text{Gd}$ nanoparticles have almost the same size, which is ~ 5 nm; there were no signs of segregation of the dopant on the surface of the crystallites, which could limit their growth. Both individual $\text{CeO}_2:\text{Gd}$ NPs and their aggregates are characterized by a fairly small size. This makes the biomedical application of such particles possible, similar to bare CeO_2 NPs.

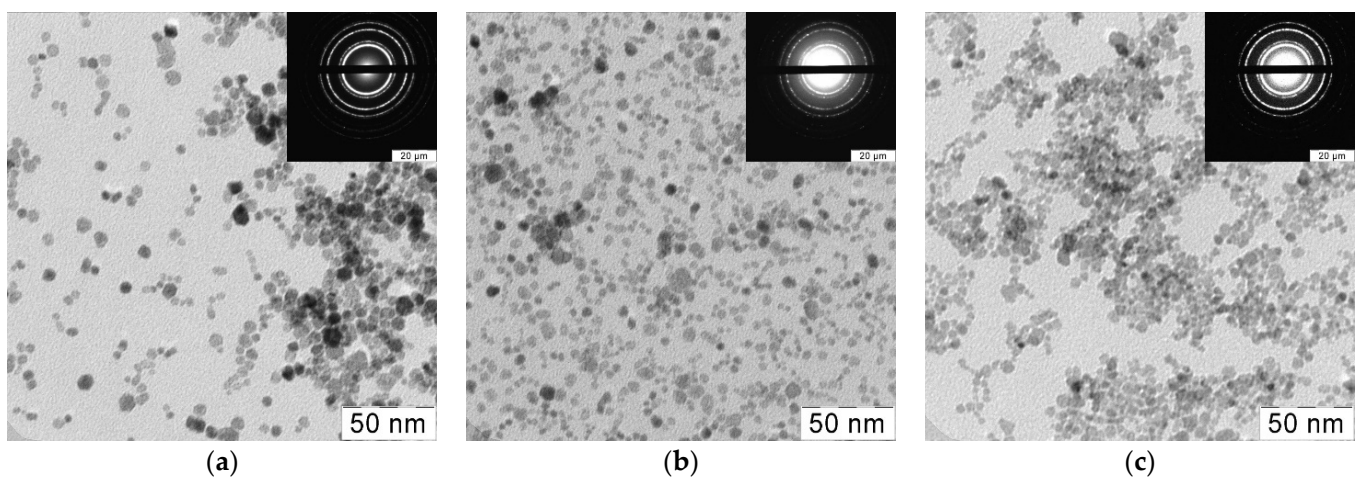


Figure 4. TEM images of CeO_2 nanoparticles with different levels of gadolinium doping (a) 0%, (b) 10%, (c) 20% (Insets: electron diffraction data).

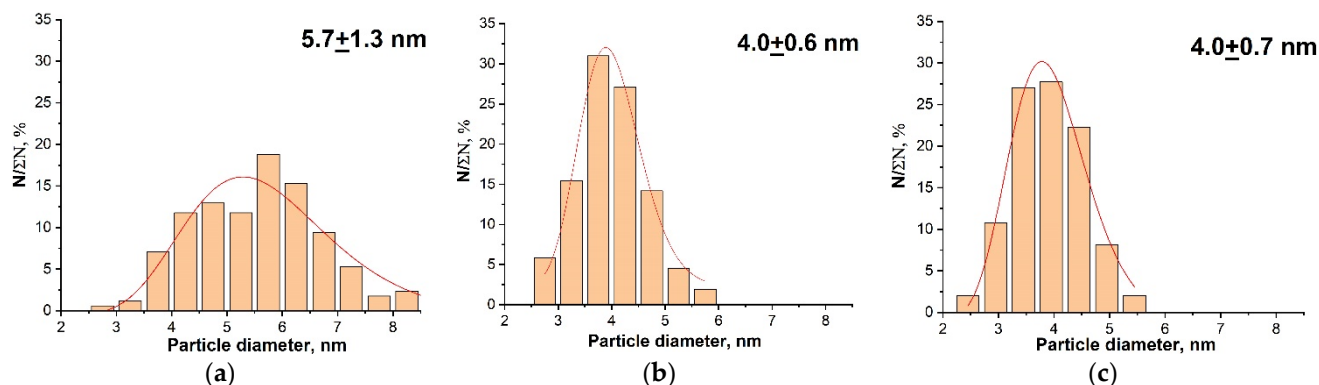


Figure 5. Particle size distributions in CeO₂ sols with different levels of gadolinium doping: (a) 0%, (b) 10%, (c) 20%.

TEM and electron diffraction data (strong ring patterns corresponding to (111) and (220) crystal planes) confirm the results of powder X-ray diffraction analysis (Figure 2a). SAED patterns did not show the presence of any impurity gadolinium phases, which is consistent with the literature data concerning gadolinium-doped ceria formation under hydrothermal conditions [33].

3.2. Enzyme-like Activity and Radical-Scavenging Properties of CeO₂ NPs and Gadolinium-Doped CeO₂ NPs

A heterovalent doping is a convenient tool for changing redox-related properties and oxygen mobility in inorganic nanomaterials. Doping nanoscale CeO₂ with trivalent lanthanides leads to modification of its biocatalytic activity and opens up wide possibilities for its tuning. In a number of recent studies, doping cerium dioxide with REE ions (Eu, Nd, Pr, La, Sm, Er) was shown to lead to an increase in the concentration of oxygen vacancies, a change in the Ce³⁺/Ce⁴⁺ ion ratio, and an increase in the catalytic activity and bioactivity of cerium dioxide [40,43]. At the same time, in some reports, a decrease in the biochemical activity of CeO₂ nanoparticles was observed when they were doped with REE ions while maintaining their high oxygen non-stoichiometry [29,71,72].

In the present study, efforts were focused on evaluating the effect of gadolinium doping on the biomimetic activity, namely SOD- and peroxidase-like activities, and the radical-scavenging properties (antioxidant activity) of nanoscale CeO₂.

3.2.1. SOD-Mimetic Activity

The SOD-like activity of nanomaterials was analyzed using the chemiluminescent method. Measurements were carried out in the presence of lucigenin, a probe sensitive to the presence of superoxide anion radicals ($\bullet\text{O}_2^-$) [73–75].

In the present study, an analysis was made of both the biochemical behavior of bare CeO₂ NPs and CeO₂:Gd NPs in relation to $\bullet\text{O}_2^-$ and the activity of the bare CeO₂ NPs and CeO₂:Gd NPs with SOD conjugates.

Figure 6a shows chemiluminograms recorded upon adding xanthine oxidase to reaction mixtures containing xanthine, lucigenin and CeO₂ sols (including Gd-doped CeO₂ sols).

The addition of xanthine oxidase to a reaction mixture containing a substrate, a chemiluminescent probe, and doped or undoped ceria sols led to the appearance of luminescence due to the formation of superoxide anion radicals. Interestingly, bare CeO₂ NPs synthesized using the ion-exchange method with subsequent hydrothermal treatment did not exhibit SOD-like activity, unlike nanoscale CeO₂ synthesized by other methods [14,15,54,55]. The enhancement of lucigenin-activated chemiluminescence, compared with the control level of luminescence (blank) in colloidal solutions containing CeO₂:Gd NPs, also indicated the absence of SOD-like activity (Figure 6a). Thus, both bare CeO₂ NPs and CeO₂:Gd NPs were pro-oxidants and contributed to the generation of reactive oxygen species (ROS).

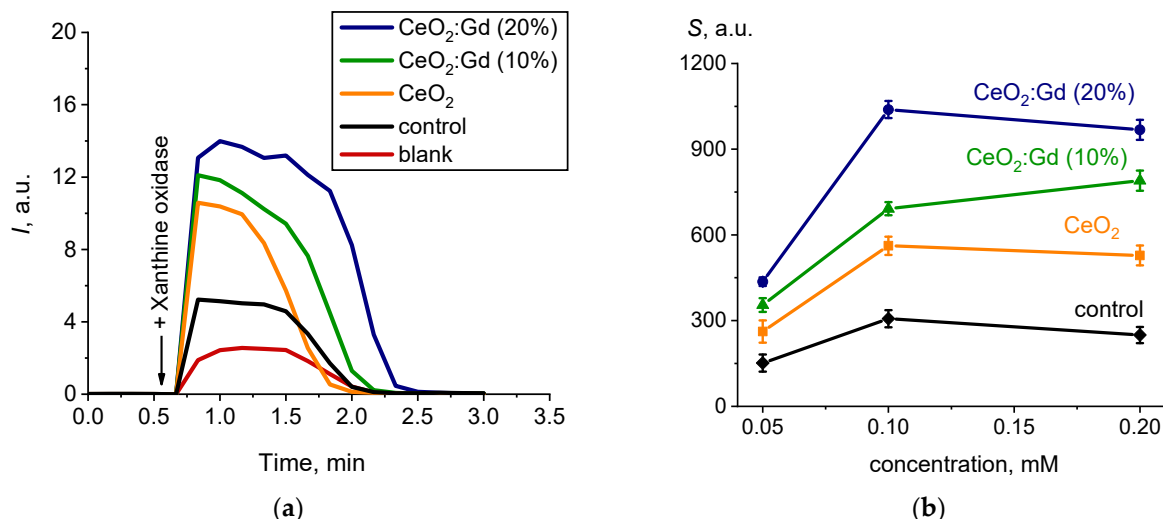


Figure 6. (a) Chemiluminograms characterizing the SOD-like activity of bare CeO₂ NPs, CeO₂:Gd NPs (10% and 20%) and a control sample; sample concentration 0.2 mM; (b) light sums (S) as a function of the concentration of samples.

Figure 6b shows the experimental dependences of the integral parameter S (the area under the chemiluminescence curve, which is proportional to the number of free radicals generated) for various concentrations of ceria sols. The relative degree of chemiluminescence suppression $\Delta S_{rel.}$ was calculated to compare the prooxidant effects inherent in ceria sols (Figure 7). The following formula was used for the calculation of $\Delta S_{rel.}$ values:

$$\Delta S_{rel.} \% = \frac{(S_0 - S)}{S_0} \times 100\%,$$

where S_0 and S are light sums (the area under the chemiluminescence curve) for the control experiment (without the addition of ceria sols) and for the experiment with ceria sols added.

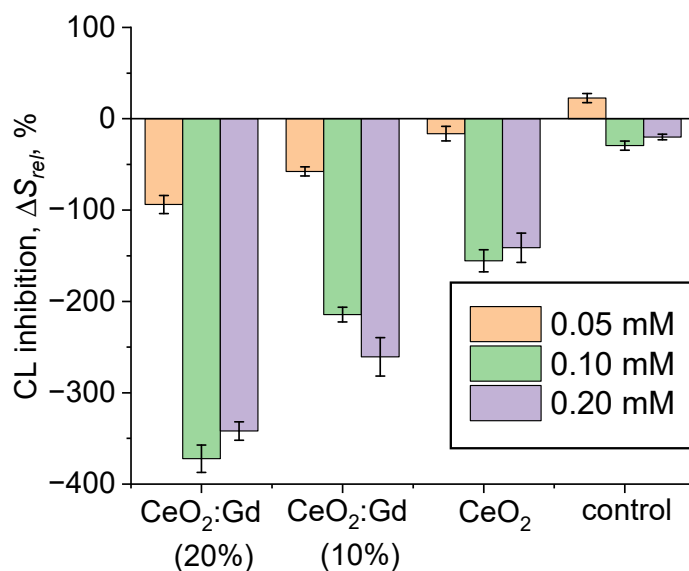


Figure 7. Histograms of the relative degrees of chemiluminescence suppression ($\Delta S_{rel.}$) for bare CeO₂ NPs, CeO₂:Gd NPs (10% and 20%) and a control sample. $\Delta S_{rel.}$ values were normalized to 100%.

The generation of ROS was enhanced in the presence of ceria sols. This effect was most pronounced in the case of CeO₂:Gd NPs (Figure 7). An increase in dopant concentration

caused an increase in the pro-oxidant properties of nanoscale CeO_2 : bare $\text{CeO}_2 < \text{CeO}_2\text{:Gd}$ (10%) $< \text{CeO}_2\text{:Gd}$ (20%).

Figure 8a shows chemiluminograms that were registered upon adding xanthine oxidase to reaction mixtures containing xanthine, lucigenin, and conjugates of $\text{CeO}_2\text{:Gd}$ NPs with SOD. According to these data, both bare CeO_2 NPs and conjugates of $\text{CeO}_2\text{:Gd}$ NPs with SOD possessed SOD-like activity (Figure 8a,b). Thus, SOD can be conjugated to gadolinium-doped CeO_2 NPs without the loss of its own enzymatic activity. Moreover, the SOD-like activity of both bare CeO_2 NPs and conjugates of $\text{CeO}_2\text{:Gd}$ NPs with SOD was less than the activity of pristine SOD (Figure 8b). Increasing the Gd concentration in nanoparticles led to a decrease in the SOD-like activity of conjugates of $\text{CeO}_2\text{:Gd}$ NPs with SOD: $\text{CeO}_2\text{-SOD} > \text{CeO}_2\text{:Gd-SOD}$ (10%) $> \text{CeO}_2\text{:Gd-SOD}$ (20%) (Figure 8b). The observed trend in changes in SOD-like properties corresponds to a concept reported in a number of earlier papers, according to which excessive dopant concentration can cause a decrease in the biocatalytic activity of nanoscale CeO_2 [76].

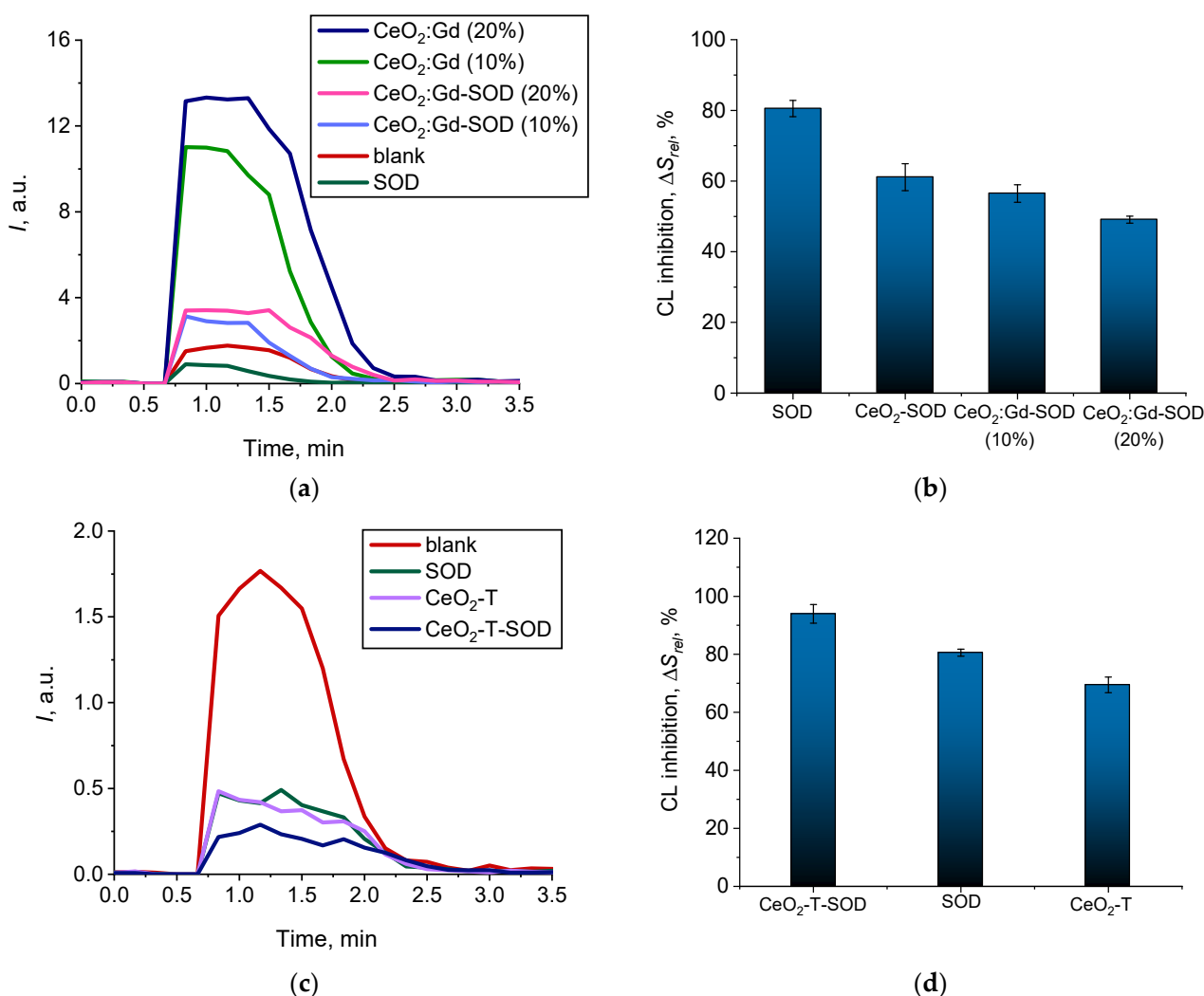


Figure 8. (a) Chemiluminograms characterizing the SOD-like activity of $\text{CeO}_2\text{:Gd}$ NPs (10% and 20%, 0.10 mM), ceria-SOD conjugates ($\text{CeO}_2\text{-SOD}$, $\text{CeO}_2\text{:Gd-SOD}$ (10%), $\text{CeO}_2\text{:Gd-SOD}$ (20%)) and SOD (10 nM); (b) histograms of the relative degrees of chemiluminescence suppression ($\Delta S_{rel.}$) for $\text{CeO}_2\text{:Gd}$ NPs, ceria-SOD conjugates and SOD; (c) chemiluminograms characterizing the SOD-like activity of citrate-stabilized CeO_2 NPs ($\text{CeO}_2\text{-T}$, 0.10 mM), ceria-SOD conjugate ($\text{CeO}_2\text{-T-SOD}$) and SOD (10 nM); (d) histograms of the relative degrees of chemiluminescence suppression ($\Delta S_{rel.}$) for citrate-stabilized CeO_2 NPs, ceria-SOD conjugate and SOD. $\Delta S_{rel.}$ values were normalized to 100%.

Since bare CeO₂ NPs obtained by the anion exchange method, contrary to expectations, did not demonstrate SOD-like activity, a citrate stabilized CeO₂ sol (the molar ratio of ceria and citrate was 1:1; particle size ~3 nm) synthesized by thermal hydrolysis of ammonium cerium(IV) nitrate was chosen as a reference sample for the preparation of conjugates with SOD [77]. Figure 8d shows chemiluminograms that were recorded for the citrate-stabilized CeO₂ sol and its conjugate with SOD.

The data obtained confirm the SOD-like activity of the citrate-stabilized CeO₂ sol (Figure 8c). The conjugate of citrate-stabilized CeO₂ NPs with SOD was characterized by more pronounced enzyme-like activity, effectively inhibiting superoxide anion radicals, compared with non-functionalized ceria (Figure 8d). This indicates a synergistic effect of citrate-stabilized CeO₂ NPs and SOD. These results correlate well with data found in the literature [54,55,78]. A number of previous studies have shown that the SOD-like activity of CeO₂ NPs increases significantly after their interaction with Cu,Zn-SOD or the electron donor molecule [Ru(dcbpy)₂(NCS)₂] [54,78]. Thus, the conjugation of CeO₂ NPs with the antioxidative enzyme is not only a means of increasing the SOD-like activity of nanoscale CeO₂ but also an effective approach to obtaining nanomaterials with tunable enzyme-like activity.

Along with functionalizing the surface of nanoscale CeO₂ with biologically active molecules, an important method for improving its biocatalytic activity involves doping CeO₂ NPs with ions of aliovalent transition and rare earth elements [33,52,62,79]. This leads to the formation of oxygen vacancies for local charge compensation. A common assumption is that, under physiological conditions, ROS can be catalytically degraded through the Ce³⁺/Ce⁴⁺ redox pair [62]. The chemical doping of nanoceria can significantly improve the catalytic activity of the Ce³⁺/Ce⁴⁺ redox pair toward biochemically relevant ROS [29,37,80]. In this regard, a high proportion of surface Ce³⁺ ions is important in the use of nanobiomaterials based on CeO₂ in the treatment of diseases caused by disturbances of redox homeostasis [80–82].

A superoxide anion radical (•O₂[−]) is one of the primary ROS formed during free radical metabolism in living organisms. The main sources of •O₂[−] in the body are mitochondria and enzymatic systems: NADPH oxidase, xanthine oxidase, lipoxygenase, and cyclooxygenase [74,83–85]. The ability to catalyze the dismutation of superoxide anion radicals was among the first types of enzyme-like activity discovered in nanocrystalline CeO₂ [14,15,86,87]. Doping CeO₂ NPs with REE ions (La³⁺, Sm³⁺, Er³⁺) was found to result in a significant increase in the SOD-like activity of nanoscale CeO₂, which was associated with an increase in the concentration of Ce³⁺ ions [43]. Presumably, the rate of inhibition of superoxide anion radicals of CeO₂ NPs doped with REE ions is closely related to the concentration of Ce³⁺ ions [33,88,89].

In a recent study, a promising endothelial protection strategy for the effective therapy of atherosclerosis through the use of CeO₂:Gd NPs was demonstrated [62]. The resulting CeO₂:Gd nanozymes combined inactivation capabilities for a broad spectrum by ROS and significantly reduced intracellular oxidative stress caused by oxidized low-density lipoprotein [62]. The effect of dopant concentration on the SOD- and catalase-like activity of nanoscale CeO₂ was studied. The improvement in the enzyme-like properties of nanoscale CeO₂ with an increase in the level of Gd doping was explained by the formation of defects in the form of oxygen vacancies and an increase in the proportion of surface Ce³⁺ ions [29,65,81]. In another study, a two-stage mechanism was proposed to explain the enhancement of the SOD-like activity of nanoscale CeO₂ with Gd doping [33]. At the first stage, the enzymatic dismutation of superoxide anion radicals occurs, with the formation of hydrogen peroxide. At the second stage, the regeneration of Ce³⁺ ions occurs, with electronic transfer and the formation of oxygen vacancies [33].

Thus, according to a widespread assumption, the biochemical activity of CeO₂ NPs, including those doped with rare earth ions, is caused exclusively by redox transitions between the Ce³⁺/Ce⁴⁺ states [14,15,90]. It should be noted, however, that the actual oxidation state of cerium in nanocrystalline CeO₂ is currently the subject of extensive

debate, since there are reasonable grounds for questioning the presence of trivalent cerium in nanoscale CeO_2 [91,92].

3.2.2. Peroxidase Mimetic Activity

The redox activity of bare CeO_2 NPs and CeO_2 :Gd NPs was analyzed in relation to one of the key molecules of free radical homeostasis, namely hydrogen peroxide. To assess the peroxidase-like activity of the samples using the chemiluminescent method, a highly sensitive analogue of luminol—8-amino-5-chloro-7-phenyl-pyrido [3,4-d]pyridazine-1,4(2*H*,3*H*)dione (L-012)—was chosen as a chemiluminescent probe molecule [57,58].

Figure 9a shows chemiluminograms that were recorded when bare CeO_2 NPs and CeO_2 :Gd NPs were added to a reaction mixture containing L-012 and H_2O_2 (pH = 7.4). In the presence of CeO_2 -based nanozymes, the luminescence intensity of the L-012 oxidation product increased.

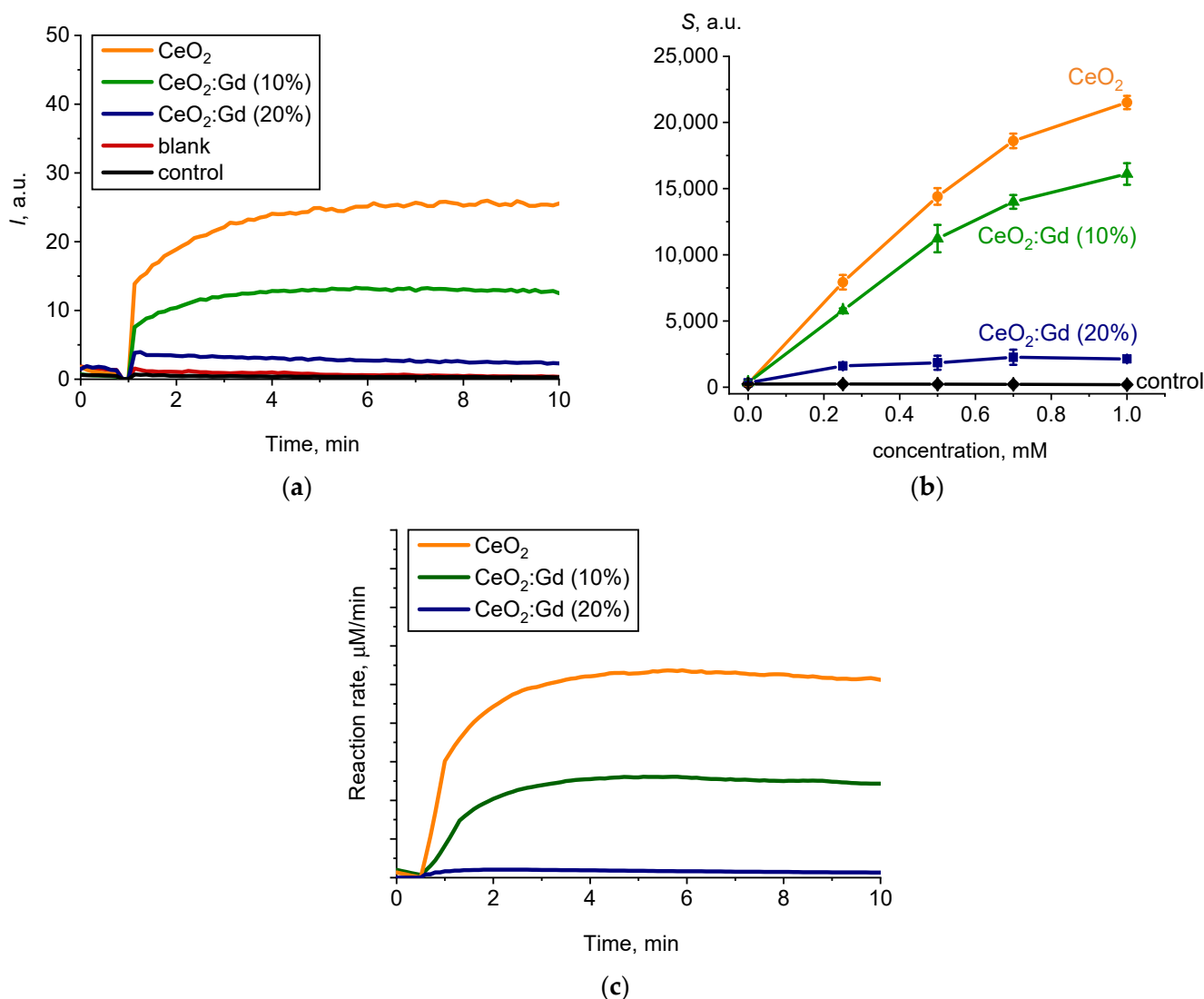


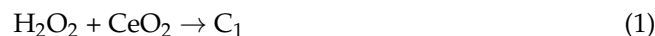
Figure 9. (a) Chemiluminograms characterizing peroxidase-like activity of the bare CeO_2 NPs, CeO_2 :Gd NPs (10% and 20%) and a control sample at pH 7.4, sample concentration 0.5 mM; (b) light sums (S) as a function of sample concentrations; (c) the results of the mathematical modeling of the corresponding chemiluminograms.

The appearance of chemiluminescence kinetic curves with a luminescence intensity reaching a stationary level enables the conclusion that the samples demonstrated

peroxidase-like properties (Figure 9a). The experimental dependences of the integral index S (the area under the chemiluminescence curve, which is proportional to the level of free radicals generated) on the concentration of the samples (Figure 9b) demonstrate the dose-dependent nature of the enhancement of chemiluminescence in the presence of CeO₂-based nanozymes. An increase in the level of Gd doping caused a decrease in the peroxidase-like activity of CeO₂ at pH = 7.4 (Figure 9b): bare CeO₂ > CeO₂:Gd (10%) > CeO₂:Gd (20%).

To confirm the enzyme mimetic property of CeO₂ NPs and to estimate the catalytic constants, the mathematical modeling of chemiluminograms was performed (Figure 9c) [55,59].

As a possible mechanism for the peroxidase-like activity of ceria nanoparticles, the following model was used:



where C₁ and C₂—reaction intermediates 1 and 2, L-012•—the oxidation product of L-012, P—chemiluminescence reaction product.

Kinetic modeling showed that the above model agrees well with the experimental data (Figure 9a,c). The estimated rate constants of reactions (1)–(4) are shown in Table 1.

Table 1. Rate constants of H₂O₂-L-012 oxidation reactions in the presence of cerium dioxide at pH = 7.4.

Sample	k_1 (μM/min)	k_2 (μM/min)	k_3 (μM/min)	k_4 (μM/min)
bare CeO ₂ NPs	3.0×10^{-14}	3.5×10^9	9.0×10^{11}	9.8×10^{-8}
CeO ₂ :Gd NPs (10%)	9.2×10^{-14}	8.7×10^9	3.8×10^{11}	3.9×10^{-8}
CeO ₂ :Gd NPs (20%)	9.0×10^{-14}	9.5×10^9	4.0×10^{11}	2.6×10^{-8}

The constant k_4 was chosen as the key kinetic parameter for comparing the peroxidase-like activity of the samples, as the chemiluminescent technique is based on the registration of the luminescence of the reaction product (Equation (4)). The data presented in Table 1 show that doping bare CeO₂ NPs with 10% and 20% Gd leads to a decrease in the catalytic activity of CeO₂ NPs toward hydrogen peroxide by 2.5 and 3.7 times, respectively.

This is consistent with the previously described assessment of the catalytic activity of CeO₂:Gd NPs toward the oxidation of hydrogen peroxide to hydroxyl radicals [29]. Doping with Gd was found to reduce the activity of catalytic sites on the surface of CeO₂ NPs. In a neutral medium (pH = 7.4), CeO₂:Gd NPs catalyzed the decomposition of H₂O₂ and the formation of •OH through a Fenton-like reaction mechanism [29]. Based on these results, the authors suggested that increasing the proportion of surface Ce³⁺ ions in CeO₂:Gd NPs could effectively increase the density and content of active sites in the NP catalyst [29]. It is important to note that Gd³⁺ dopants are not directly involved in the oxidation of H₂O₂, due to the high stability of the Gd³⁺ oxidation state [29]. The tendency for catalytic activity to decrease with increasing dopant concentration in CeO₂:Gd NPs was also observed in a study of the scavenging activity of nanoscale CeO₂ against hydroxyl radicals [72]. It was suggested that the redox inactivity of gadolinium(III) in the crystal lattice of nanoscale CeO₂ slows the redox cycling of Ce³⁺/Ce⁴⁺, causing a deterioration in the antioxidant properties of CeO₂:Gd NPs [72]. These data are confirmed by other reports, in which researchers explain such a dependence as being the result of the formation of stable oxygen vacancy defect complexes [41].

Figure 10a shows chemiluminograms recorded when bare CeO₂ NPs and CeO₂:Gd NPs were added to a reaction mixture containing L-012 and H₂O₂ (pH = 8.6).

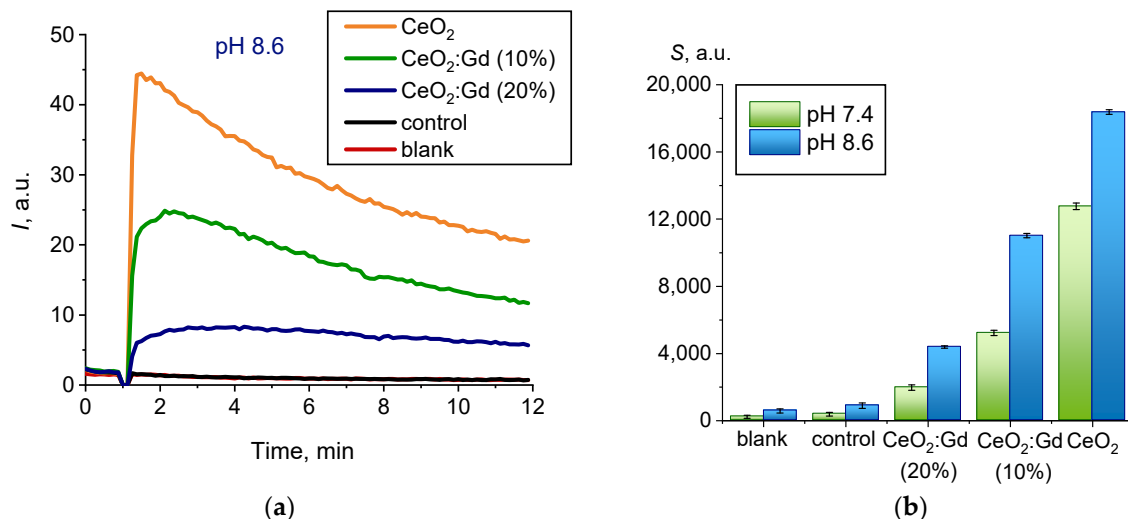


Figure 10. (a) Chemiluminograms characterizing peroxidase-like activity of the bare CeO₂ NPs and CeO₂:Gd NPs (10% and 20%) at pH = 8.6, sample concentration 0.5 mM; (b) corresponding dependencies of light sums (*S*) at pH = 7.4 and 8.6.

The appearance of the chemiluminescence kinetic curves suggests that, at pH = 8.6, bare CeO₂ NPs and CeO₂:Gd NPs (Figure 10a) demonstrate non-peroxidase-like activity toward hydrogen peroxide, when compared with the results obtained at pH = 7.4 (Figure 9a). Trends in changes in the biochemical activity of CeO₂ nanoparticles caused by doping with gadolinium remained unchanged at all pH values studied (Figure 10b): bare CeO₂ > CeO₂:Gd (10%) > CeO₂:Gd (20%).

It is known that nanoscale CeO₂ in biological systems can exhibit both pro- and antioxidant activity toward hydrogen peroxide [59,93]. This is also typical for CeO₂:Gd NPs. In a number of studies, it was found that CeO₂:Gd NPs exhibit predominantly catalase-like activity toward hydrogen peroxide [39,62]. With increasing dopant concentration, the catalase-like properties of CeO₂:Gd NPs have been found to increase [62]. The pH is one factor that significantly affects the balance of the pro- and antioxidant properties of CeO₂ NPs. A similar pH dependence of biochemical activity has been found for CeO₂ nanoparticles doped with Gd [39]. For example, for PEGylated Yb₂O₃:Gd@SiO₂@CeO₂, it has been shown that pH = 4.0 is the most optimal pH for the manifestation of catalase-like properties [39]. This is consistent with the data published earlier for bare CeO₂ NPs [19,39].

It is particularly important to emphasize that, currently, the enzyme-like nature of the catalytic activity of inorganic nanomaterials is being questioned. A growing number of publications are highlighting the need to reconsider the correctness of using the formalism of enzymatic reactions when describing the activity of nanomaterials with respect to various model substrates [94,95]. All of the abovementioned issues definitely require systematic research based on methods and approaches used in enzymology and the kinetic analysis of reactions.

3.2.3. Radical-Scavenging Properties (Antioxidant Activity)

The radical-scavenging properties (antioxidant activity) of bare CeO₂ NPs and CeO₂:Gd NPs were analyzed in relation to organic radicals, namely alkylperoxyl radicals. The corresponding chemiluminograms of ceria sols are presented in Figure 11a. Note that, in Figure 11a, ceria samples possess different reaction kinetics. When bare CeO₂ NPs and CeO₂:Gd NPs (10%) were added, the luminescence level decreased to zero and then gradually increased (green and orange lines in Figure 11). Upon the addition of CeO₂:Gd NPs (20%), the luminescence intensity instantly recovered to a reasonable level, which was lower than that of a blank. The differences in the rate of the restoration of luminescence intensity reflect the different radical-scavenging properties of the nanoparticles.

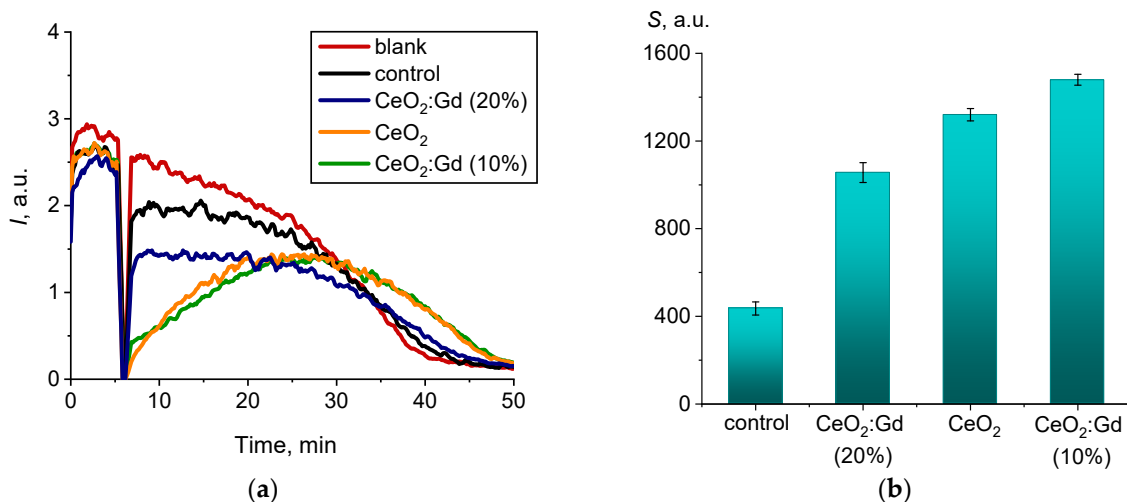


Figure 11. (a) Chemiluminograms characterizing the radical-scavenging properties of bare CeO₂ NPs, CeO₂:Gd NPs (10% and 20%) and a control sample, (sample concentrations 1.5 mM); (b) histograms of chemiluminescence suppression (S_{CL} , a.u.) for ceria sols.

When bare CeO₂ NPs and CeO₂:Gd NPs interact with alkylperoxyl radicals in the presence of luminol, a decrease in luminescence intensity is observed. The different time dependences of chemiluminescence intensity indicate different values of the rate constants relating to the interaction of CeO₂-based nanozymes with radicals [96]. The lowest degree of luminescence suppression was associated with the CeO₂ sol doped with 20% Gd (Figure 11a). This effect is characteristic of weak antioxidants whose rate constant of radical scavenging is less than the rate constant of the interaction of radicals with luminol [96]. In turn, CeO₂ sol with less Gd doping (10%) showed more pronounced antioxidant activity, which is characteristic of medium-strength antioxidants. The use of mathematical modeling in the study showed that the values of the rate constants for the interaction of medium-strength antioxidants with radicals were close to the value of the rate constant for luminol [96].

The area of the luminescence suppression region (S_{CL} , a.u.) was calculated from chemiluminograms to quantitatively characterize the radical-scavenging properties of the sols, reflecting antioxidant capacity as defined by the degree of luminescence suppression, which is proportional to the number of scavenged radicals (Figure 11b). Both bare CeO₂ sol and CeO₂ sol doped with Gd (10%) demonstrated the most pronounced antioxidant properties against alkylperoxyl radicals. An increase in the dopant content to 20% led to a decrease in the radical-scavenging properties of nanodispersed cerium dioxide. A similar effect, whereby an excessive dopant concentration can cause a decrease in the biocatalytic activity of CeO₂ nanoparticles, has been reported in some previous works [76].

3.3. Analysis of the Biological Activity of CeO₂ and Gadolinium Doped (20%) CeO₂ Sols, Including Sols Stabilized with Maltodextrin and Citrate Ions

One of the key factors for assessing the prospects for biomedical applications of engineered nanomaterials is their biological activity and the absence of toxicity. In this regard, the research team conducted an analysis of the biological activity and an assessment of the toxicity of aqueous sols of cerium dioxide, including sols doped with gadolinium (with a maximum doping level of 20%). Similar sols containing ammonium citrate (Cit) and maltodextrin (M)—stabilizers widely used in biomedical applications—were also analyzed. The concentration of stabilizers was taken in a twofold molar excess relative to the concentration of cerium oxide. The materials and methods for these measurements are presented in detail in Supplementary Materials.

According to the data obtained, CeO₂ NPs or CeO₂:Gd NPs (20%), including those stabilized with maltodextrin or ammonium citrate, had a high degree of biocompatibility in a culture of mouse fibroblast cells of the NCTC L929 line, as confirmed by a high level

of mitochondrial membrane potential, high metabolic activity, and a low percentage of non-viable cells after 24 h of incubation, in a wide range of ceria-based sol concentrations (0.001–0.5 mg/mL) (Figures S1–S5, Supplementary Materials).

The high degree of biocompatibility of the synthesized ceria sols correlates well with previously obtained data on the high degree of biocompatibility of cerium-containing nanomaterials both in vitro [97] and in vivo [98].

4. Conclusions

In this study, stable colloids of bare CeO₂ NPs and CeO₂:Gd NPs containing various concentrations of gadolinium (10 mol.% or 20 mol.%) were synthesized. Unexpectedly, neither the bare CeO₂ NPs nor the CeO₂:Gd NPs demonstrated SOD-like activity, while they acted as prooxidants and contributed to the generation of ROSs. Gadolinium doping increased the prooxidant properties of nanocrystalline ceria. At the same time, conjugates of bare CeO₂ NPs and CeO₂:Gd NPs with SOD exhibited SOD-like activity. The SOD-like activity of the conjugates increased with a decrease in the gadolinium content in nanoscale CeO₂.

In contrast to SOD-like properties, peroxidase-like activity was inherent in both bare CeO₂ NPs and CeO₂:Gd NPs. This type of enzyme-like activity was found to be pH-dependent. In neutral media (pH 7.4), nanoscale CeO₂ acted as a prooxidant enzyme (peroxidase), while in slightly alkaline media (pH = 8.6), it lost its catalytic properties and thus cannot be regarded as a nanozyme. The peroxidase-like activity of nanoscale CeO₂ increased with a decrease in gadolinium content.

Both CeO₂ NPs and CeO₂:Gd NPs demonstrated radical-scavenging properties toward organic (alkylperoxy) radicals. The level of doping of nanoscale CeO₂ with gadolinium affected the kinetics of the interaction of CeO₂ NPs with alkylperoxy radicals. Nanoscale CeO₂ with a 10% Gd doping level acted as an antioxidant of medium strength, while nanoscale CeO₂ with a 20% Gd doping level acted as a weak antioxidant (antioxidant of prolonged action).

Thus, doping nanoscale CeO₂ with gadolinium and conjugation with SOD can be convenient tools for fine-tuning the biochemical behavior of CeO₂ NPs. The data obtained can contribute to understanding the mechanisms responsible for the multifaceted nanozyme activity of CeO₂ NPs and expand the possibilities for their biomedical application.

Supplementary Materials: The following supporting information can be downloaded at: <https://www.mdpi.com/article/10.3390/nano14090769/s1>, Figure S1. Assessment of the dehydrogenase activity level of NCTC L929 cells after 24 h of cultivation with bare CeO₂ NPs or CeO₂:Gd NPs (20%), including those stabilised with maltodextrin or ammonium citrate. Data are presented as M ± SD. The reliability of the results was calculated using the Mann-Whitney U test at $p < 0.05$. Figure S2. Microimages of the NCTC cell line L929 after staining with a mixture of dyes SYTO 9 (green)/propidium iodide (red) after 24 h of cultivation with bare CeO₂ NPs, including those containing maltodextrin or ammonium citrate. The concentration is expressed in mg/mL. Scale bar is 100 microns. Figure S3. Microimages of the NCTC cell line L929 after staining with a mixture of dyes SYTO 9 (green)/propidium iodide (red) after 24 h of cultivation with CeO₂:Gd NPs (20%), including those stabilised with maltodextrin or ammonium citrate. The concentration is expressed in mg/mL. Scale bar is 100 microns. Figure S4. Microimages of the NCTC cell line L929 after staining with tetramethylrhodamine (TMRE) after 24 h of cultivation with bare CeO₂ NPs, including those stabilised with maltodextrin or ammonium citrate. Scale bar is 100 microns. Figure S5. Microimages of the NCTC cell line L929 after staining with tetramethylrhodamine (TMRE) after 24 h of cultivation with CeO₂:Gd NPs (20%), including those stabilised with maltodextrin or ammonium citrate. Scale bar is 100 microns. Ref. [99] is cited in the Supplementary Materials.

Author Contributions: Conceptualization, V.K.I.; Methodology, M.M.S., T.O.K. and A.L.P.; Validation, M.M.S.; Formal analysis, M.M.S.; Investigation, T.O.K., T.S.B., D.D.K., D.A.V., O.S.I. and A.V.L.; Resources, M.M.S., T.O.K., A.L.P., A.V.L. and A.E.B.; Data curation, M.M.S. and T.O.K.; Writing—original draft, A.L.P.; Writing—review & editing, A.E.B. and V.K.I.; Visualization, D.D.K.;

Supervision, A.E.B. and V.K.I.; Project administration, A.L.P.; Funding acquisition, A.L.P. All authors have read and agreed to the published version of the manuscript.

Funding: This work was supported by the Russian Science Foundation [grant agreement No. 22-73-10231], <https://www.rscf.ru/project/22-73-10231/> (accessed on 23 April 2024).

Data Availability Statement: Data are contained within the article and Supplementary Materials.

Conflicts of Interest: The authors declare no conflict of interest.

References

1. Li, D.; Fan, T.; Mei, X. A Comprehensive Exploration of the Latest Innovations for Advancements in Enhancing Selectivity and Efficiency of Nanozymes for Theranostic Nanoplatfoms. *Nanoscale* **2023**, *15*, 15885–15905. [[CrossRef](#)] [[PubMed](#)]
2. Singh, H.; Sareen, D.; George, J.M.; Bhardwaj, V.; Rha, S.; Lee, S.J.; Sharma, S.; Sharma, A.; Kim, J.S. Mitochondria targeted fluorogenic theranostic agents for cancer therapy. *Coord. Chem. Rev.* **2022**, *452*, 214283. [[CrossRef](#)]
3. Muráth, S.; Szerlauth, A.; Sebők, D.; Szilágyi, I. Layered double hydroxide nanoparticles to overcome the hydrophobicity of ellagic acid: An antioxidant hybrid material. *Antioxidants* **2020**, *9*, 153. [[CrossRef](#)]
4. Eriksson, P.; Tal, A.A.; Skallberg, A.; Brommesson, C.; Hu, Z.; Boyd, R.D.; Olovsson, W.; Fairley, N.; Abrikosov, I.A.; Zhang, X. Cerium oxide nanoparticles with antioxidant capabilities and gadolinium integration for MRI contrast enhancement. *Sci. Rep.* **2018**, *8*, 6999. [[CrossRef](#)] [[PubMed](#)]
5. Marte, B. Tumour heterogeneity. *Nature* **2013**, *501*, 327. [[CrossRef](#)] [[PubMed](#)]
6. Alizadeh, A.A.; Aranda, V.; Bardelli, A.; Blanpain, C.; Bock, C.; Borowski, C.; Caldas, C.; Califano, A.; Doherty, M.; Elsner, M. Toward understanding and exploiting tumor heterogeneity. *Nat. Med.* **2015**, *21*, 846–853. [[CrossRef](#)] [[PubMed](#)]
7. Zhang, Y.; Jin, Y.; Cui, H.; Yan, X.; Fan, K. Nanozyme-based catalytic theranostics. *RSC Adv.* **2020**, *10*, 10–20. [[CrossRef](#)] [[PubMed](#)]
8. Ali, A.; Ovais, M.; Zhou, H.; Rui, Y.; Chen, C. Tailoring metal-organic frameworks-based nanozymes for bacterial theranostics. *Biomaterials* **2021**, *275*, 120951. [[CrossRef](#)] [[PubMed](#)]
9. Jiang, D.; Ni, D.; Rosenkrans, Z.T.; Huang, P.; Yan, X.; Cai, W. Nanozyme: New horizons for responsive biomedical applications. *Chem. Soc. Rev.* **2019**, *48*, 3683–3704. [[CrossRef](#)]
10. Foulkes, R.; Man, E.; Thind, J.; Yeung, S.; Joy, A.; Hoskins, C. The regulation of nanomaterials and nanomedicines for clinical application: Current and future perspectives. *Biomater. Sci.* **2020**, *8*, 4653–4664. [[CrossRef](#)]
11. Celardo, I.; Pedersen, J.Z.; Traversa, E.; Ghibelli, L. Pharmacological potential of cerium oxide nanoparticles. *Nanoscale* **2011**, *3*, 1411–1420. [[CrossRef](#)] [[PubMed](#)]
12. Popov, A.L.; Shcherbakov, A.B.; Zholobak, N.; Baranchikov, A.Y.; Ivanov, V.K. Cerium dioxide nanoparticles as third-generation enzymes (nanozymes). *Nanosyst. Phys. Chem. Math.* **2017**, *8*, 760–781. [[CrossRef](#)]
13. Shcherbakov, A.B.; Reukov, V.V.; Yakimansky, A.V.; Krasnopeeva, E.L.; Ivanova, O.S.; Popov, A.L.; Ivanov, V.K. CeO₂ nanoparticle-containing polymers for biomedical applications: A review. *Polymers* **2021**, *13*, 924. [[CrossRef](#)]
14. Korsvik, C.; Patil, S.; Seal, S.; Self, W.T. Superoxide dismutase mimetic properties exhibited by vacancy engineered ceria nanoparticles. *Chem. Commun.* **2007**, 1056–1058. [[CrossRef](#)] [[PubMed](#)]
15. Heckert, E.G.; Karakoti, A.S.; Seal, S.; Self, W.T. The role of cerium redox state in the SOD mimetic activity of nanoceria. *Biomaterials* **2008**, *29*, 2705–2709. [[CrossRef](#)] [[PubMed](#)]
16. Baldim, V.; Bedioui, F.; Mignet, N.; Margail, I.; Berret, J.-F. The enzyme-like catalytic activity of cerium oxide nanoparticles and its dependency on Ce³⁺ surface area concentration. *Nanoscale* **2018**, *10*, 6971–6980. [[CrossRef](#)] [[PubMed](#)]
17. Sozarukova, M.M.; Shestakova, M.A.; Teplonogova, M.A.; Izmailov, D.Y.; Proskurnina, E.V.; Ivanov, V.K. Quantification of free radical scavenging properties and SOD-like activity of cerium dioxide nanoparticles in biochemical models. *Russ. J. Inorg. Chem.* **2020**, *65*, 597–605. [[CrossRef](#)]
18. Singh, R.; Singh, S. Role of phosphate on stability and catalase mimetic activity of cerium oxide nanoparticles. *Colloids Surf. B Biointerfaces* **2015**, *132*, 78–84. [[CrossRef](#)]
19. Pirmohamed, T.; Dowding, J.M.; Singh, S.; Wasserman, B.; Heckert, E.; Karakoti, A.S.; King, J.E.; Seal, S.; Self, W.T. Nanoceria exhibit redox state-dependent catalase mimetic activity. *Chem. Commun.* **2010**, *46*, 2736–2738. [[CrossRef](#)]
20. Singh, R.; Singh, S. Redox-dependent catalase mimetic cerium oxide-based nanozyme protect human hepatic cells from 3-AT induced acatalasemia. *Colloids Surf. B Biointerfaces* **2019**, *175*, 625–635. [[CrossRef](#)]
21. Jiao, X.; Song, H.; Zhao, H.; Bai, W.; Zhang, L.; Lv, Y. Well-redispersed ceria nanoparticles: Promising peroxidase mimetics for H₂O₂ and glucose detection. *Anal. Methods* **2012**, *4*, 3261–3267. [[CrossRef](#)]
22. Ansari, A.A.; Solanki, P.R.; Malhotra, B. Hydrogen peroxide sensor based on horseradish peroxidase immobilized nanostructured cerium oxide film. *J. Biotechnol.* **2009**, *142*, 179–184. [[CrossRef](#)] [[PubMed](#)]
23. Asati, A.; Santra, S.; Kaittanis, C.; Nath, S.; Perez, J.M. Oxidase-like activity of polymer-coated cerium oxide nanoparticles. *Angew. Chem.* **2009**, *121*, 2344–2348. [[CrossRef](#)] [[PubMed](#)]
24. Asati, A.; Kaittanis, C.; Santra, S.; Perez, J.M. pH-tunable oxidase-like activity of cerium oxide nanoparticles achieving sensitive fluorogenic detection of cancer biomarkers at neutral pH. *Anal. Chem.* **2011**, *83*, 2547–2553. [[CrossRef](#)] [[PubMed](#)]

25. Liu, B.; Huang, Z.; Liu, J. Boosting the oxidase mimicking activity of nanoceria by fluoride capping: Rivaling protein enzymes and ultrasensitive F^- detection. *Nanoscale* **2016**, *8*, 13562–13567. [[CrossRef](#)] [[PubMed](#)]
26. Tian, Z.; Yao, T.; Qu, C.; Zhang, S.; Li, X.; Qu, Y. Photolyase-like catalytic behavior of CeO_2 . *Nano Lett.* **2019**, *19*, 8270–8277. [[CrossRef](#)] [[PubMed](#)]
27. Khulbe, K.; Karmakar, K.; Ghosh, S.; Chandra, K.; Chakravorty, D.; Mugesh, G. Nanoceria-based phospholipase-mimetic cell membrane disruptive antibiofilm agents. *ACS Appl. Bio Mater.* **2020**, *3*, 4316–4328. [[CrossRef](#)]
28. Xu, F.; Lu, Q.; Huang, P.-J.J.; Liu, J. Nanoceria as a DNase I mimicking nanozyme. *Chem. Commun.* **2019**, *55*, 13215–13218. [[CrossRef](#)]
29. Bhalkikar, A.; Wu, T.-S.; Fisher, T.J.; Sarella, A.; Zhang, D.; Gao, Y.; Soo, Y.-L.; Cheung, C.L. Tunable catalytic activity of gadolinium-doped ceria nanoparticles for pro-oxidation of hydrogen peroxide. *Nano Res.* **2020**, *13*, 2384–2392. [[CrossRef](#)]
30. Sozarukova, M.M.; Proskurnina, E.V.; Popov, A.L.; Kalinkin, A.L.; Ivanov, V.K. New facets of nanozyme activity of ceria: Lipid and phospholipoperoxidase-like behaviour of CeO_2 nanoparticles. *RSC Adv.* **2021**, *11*, 35351–35360. [[CrossRef](#)]
31. Liu, D.; Yang, P.; Wang, F.; Wang, C.; Chen, L.; Ye, S.; Dramou, P.; Chen, J.; He, H. Study on performance of mimic uricase and its application in enzyme-free analysis. *Anal. Bioanal. Chem.* **2021**, *413*, 6571–6580. [[CrossRef](#)]
32. Alpaslan, E.; Yazici, H.; Golshan, N.H.; Ziemer, K.S.; Webster, T.J. pH-dependent activity of dextran-coated cerium oxide nanoparticles on prohibiting osteosarcoma cell proliferation. *ACS Biomater. Sci. Eng.* **2015**, *1*, 1096–1103. [[CrossRef](#)] [[PubMed](#)]
33. Shi, X.; Yang, J.; Wen, X.; Tian, F.; Li, C. Oxygen vacancy enhanced biomimetic superoxide dismutase activity of CeO_2 -Gd nanozymes. *J. Rare Earths* **2021**, *39*, 1108–1116. [[CrossRef](#)]
34. Li, C.; Shi, X.; Bao, L.; Yang, J.; Damirin, A.; Zhang, J. The correlation between multiple variable factors and the autocatalytic properties of cerium oxide nanoparticles based on cell viability. *New J. Chem.* **2018**, *42*, 9975–9986. [[CrossRef](#)]
35. Neal, C.J.; Kolanthai, E.; Wei, F.; Coathup, M.; Seal, S. Surface Chemistry of Biologically-Active Reducible Oxide Nanozymes. *Adv. Mater.* **2023**, *36*, 2211261. [[CrossRef](#)] [[PubMed](#)]
36. Kumar, A.; Devanathan, R.; Shutthanandan, V.; Kuchibhatla, S.; Karakoti, A.; Yong, Y.; Thevuthasan, S.; Seal, S. Radiation-induced reduction of ceria in single and polycrystalline thin films. *J. Phys. Chem. C* **2012**, *116*, 361–366. [[CrossRef](#)]
37. Wu, Y.; Xu, W.; Jiao, L.; Tang, Y.; Chen, Y.; Gu, W.; Zhu, C. Defect engineering in nanozymes. *Mater. Today* **2022**, *52*, 327–347. [[CrossRef](#)]
38. Wei, Z.; Wu, M.; Li, Z.; Lin, Z.; Zeng, J.; Sun, H.; Liu, X.; Liu, J.; Li, B.; Zeng, Y. Gadolinium-doped hollow CeO_2 - ZrO_2 nanoplatform as multifunctional MRI/CT dual-modal imaging agent and drug delivery vehicle. *Drug Deliv.* **2018**, *25*, 353–363. [[CrossRef](#)] [[PubMed](#)]
39. Li, J.; Yao, S.; Song, S.; Wang, X.; Wang, Y.; Ding, X.; Wang, F.; Zhang, H. Designed synthesis of multi-functional PEGylated Yb_2O_3 :Gd@ SiO_2 @ CeO_2 islands core@shell nanostructure. *Dalton Trans.* **2016**, *45*, 11522–11527. [[CrossRef](#)]
40. Vinothkumar, G.; Rengaraj, S.; Arunkumar, P.; Cha, S.W.; Suresh Babu, K. Ionic radii and concentration dependency of RE^{3+} (Eu^{3+} , Nd^{3+} , Pr^{3+} , and La^{3+})-doped cerium oxide nanoparticles for enhanced multienzyme-mimetic and hydroxyl radical scavenging activity. *J. Phys. Chem. C* **2018**, *123*, 541–553. [[CrossRef](#)]
41. Ackermann, S.; Sauvin, L.; Castiglioni, R.; Rupp, J.L.; Scheffe, J.R.; Steinfeld, A. Kinetics of CO_2 reduction over nonstoichiometric ceria. *J. Phys. Chem. C* **2015**, *119*, 16452–16461. [[CrossRef](#)] [[PubMed](#)]
42. Babu, S.; Thanneeru, R.; Inerbaev, T.; Day, R.; Masunov, A.E.; Schulte, A.; Seal, S. Dopant-mediated oxygen vacancy tuning in ceria nanoparticles. *Nanotechnology* **2009**, *20*, 085713. [[CrossRef](#)] [[PubMed](#)]
43. Gupta, A.; Das, S.; Neal, C.J.; Seal, S. Controlling the surface chemistry of cerium oxide nanoparticles for biological applications. *J. Mater. Chem. B* **2016**, *4*, 3195–3202. [[CrossRef](#)] [[PubMed](#)]
44. Todd, D.J.; Kay, J. Nephrogenic systemic fibrosis: An epidemic of gadolinium toxicity. *Curr. Rheumatol. Rep.* **2008**, *10*, 195–204. [[CrossRef](#)]
45. Rogosnitzky, M.; Branch, S. Gadolinium-based contrast agent toxicity: A review of known and proposed mechanisms. *Biomaterials* **2016**, *29*, 365–376. [[CrossRef](#)]
46. Söderlind, F.; Pedersen, H.; Petoral, R.M., Jr.; Käll, P.-O.; Uvdal, K. Synthesis and characterisation of Gd_2O_3 nanocrystals functionalised by organic acids. *J. Colloid Interface Sci.* **2005**, *288*, 140–148. [[CrossRef](#)] [[PubMed](#)]
47. Ahrén, M.; Selegård, L.; Söderlind, F.; Linares, M.; Kauczor, J.; Norman, P.; Käll, P.-O.; Uvdal, K. A simple polyol-free synthesis route to Gd_2O_3 nanoparticles for MRI applications: An experimental and theoretical study. *J. Nanoparticle Res.* **2012**, *14*, 1006. [[CrossRef](#)]
48. Ahrén, M.; Selegård, L.; Klasson, A.; Soderlind, F.; Abrikosova, N.; Skoglund, C.; Bengtsson, T.; Engström, M.; Käll, P.O.; Uvdal, K. Synthesis and characterization of PEGylated Gd_2O_3 nanoparticles for MRI contrast enhancement. *Langmuir* **2010**, *26*, 5753–5762. [[CrossRef](#)]
49. Hu, Z.; Ahrén, M.; Selegård, L.; Skoglund, C.; Söderlind, F.; Engström, M.; Zhang, X.; Uvdal, K. Highly Water-Dispersible Surface-Modified Gd_2O_3 Nanoparticles for Potential Dual-Modal Bioimaging. *Chem. Eur. J.* **2013**, *19*, 12658–12667. [[CrossRef](#)]
50. Nune, S.K.; Gunda, P.; Thallapally, P.K.; Lin, Y.-Y.; Laird Forrest, M.; Berkland, C.J. Nanoparticles for biomedical imaging. *Expert Opin. Drug Deliv.* **2009**, *6*, 1175–1194. [[CrossRef](#)]
51. Sharma, P.; Brown, S.; Walter, G.; Santra, S.; Moudgil, B. Nanoparticles for bioimaging. *Adv. Colloid Interface Sci.* **2006**, *123*, 471–485. [[CrossRef](#)] [[PubMed](#)]
52. Popov, A.; Abakumov, M.; Savintseva, I.; Ermakov, A.; Popova, N.; Ivanova, O.; Kolmanovich, D.; Baranchikov, A.; Ivanov, V. Biocompatible dextran-coated gadolinium-doped cerium oxide nanoparticles as MRI contrast agents with high T_1 relaxivity and selective cytotoxicity to cancer cells. *J. Mater. Chem. B* **2021**, *9*, 6586–6599. [[CrossRef](#)] [[PubMed](#)]
53. Gasymova, G.A.; Ivanova, O.S.; Baranchikov, A.Y.; Shcherbakov, A.B.; Ivanov, V.K.; Tret'yakov, Y.D. Synthesis of aqueous sols of nanocrystalline ceria doped with gadolinia. *Nanosyst. Phys. Chem. Math.* **2011**, *2*, 113–120.
54. Gil, D.; Rodriguez, J.; Ward, B.; Vertegel, A.; Ivanov, V.; Reukov, V. Antioxidant activity of SOD and catalase conjugated with nanocrystalline ceria. *Bioengineering* **2017**, *4*, 18. [[CrossRef](#)]

55. Sozarukova, M.M.; Proskurnina, E.V.; Baranchikov, A.E.; Ivanov, V.K. CeO₂ nanoparticles as free radical regulators in biological systems. *Nanosyst. Phys. Chem. Math.* **2020**, *11*, 324–332. [[CrossRef](#)]
56. Fridovich, I. Quantitative aspects of the production of superoxide anion radical by milk xanthine oxidase. *J. Biol. Chem.* **1970**, *245*, 4053–4057. [[CrossRef](#)] [[PubMed](#)]
57. Ichibangase, T.; Ohba, Y.; Kishikawa, N.; Nakashima, K.; Kuroda, N. Evaluation of lophine derivatives as L-012 (luminol analog)-dependent chemiluminescence enhancers for measuring horseradish peroxidase and H₂O₂. *Luminescence* **2014**, *29*, 118–121. [[CrossRef](#)] [[PubMed](#)]
58. Zhang, W.; Hao, L.; Huang, J.; Xia, L.; Cui, M.; Zhang, X.; Gu, Y.; Wang, P. Chemiluminescence chitosan hydrogels based on the luminol analog L-012 for highly sensitive detection of ROS. *Talanta* **2019**, *201*, 455–459. [[CrossRef](#)] [[PubMed](#)]
59. Filippova, A.D.; Sozarukova, M.M.; Baranchikov, A.E.; Kottsov, S.Y.; Cherednichenko, K.A.; Ivanov, V.K. Peroxidase-like Activity of CeO₂ Nanozymes: Particle Size and Chemical Environment Matter. *Molecules* **2023**, *28*, 3811. [[CrossRef](#)]
60. Alekseev, A.V.; Proskurnina, E.V.; Vladimirov, Y.A. Determination of antioxidants by sensitized chemiluminescence using 2, 2'-azo-bis (2-amidinopropane). *Mosc. Univ. Chem. Bull.* **2012**, *67*, 127–132. [[CrossRef](#)]
61. Yin, L.; Wang, Y.; Pang, G.; Koltypin, Y.; Gedanken, A. Sonochemical synthesis of cerium oxide nanoparticles—Effect of additives and quantum size effect. *J. Colloid Interface Sci.* **2002**, *246*, 78–84. [[CrossRef](#)] [[PubMed](#)]
62. Gao, Y.; Liu, S.; Zeng, X.; Guo, Z.; Chen, D.; Li, S.; Tian, Z.; Qu, Y. Reduction of Reactive Oxygen Species Accumulation Using Gadolinium-Doped Ceria for the Alleviation of Atherosclerosis. *ACS Appl. Mater. Interfaces* **2023**, *15*, 10414–10425. [[CrossRef](#)] [[PubMed](#)]
63. Li, J.G.; Ikegami, T.; Wang, Y.; Mori, T. 10-mol%-Gd₂O₃-Doped CeO₂ solid solutions via carbonate coprecipitation: A comparative study. *J. Am. Ceram. Soc.* **2003**, *86*, 915–921. [[CrossRef](#)]
64. Mehmood, R.; Ariotti, N.; Yang, J.L.; Koshy, P.; Sorrell, C.C. pH-responsive morphology-controlled redox behavior and cellular uptake of nanoceria in fibrosarcoma. *ACS Biomater. Sci. Eng.* **2018**, *4*, 1064–1072. [[CrossRef](#)] [[PubMed](#)]
65. Dong, S.; Dong, Y.; Liu, B.; Liu, J.; Liu, S.; Zhao, Z.; Li, W.; Tian, B.; Zhao, R.; He, F. Guiding Transition Metal-Doped Hollow Cerium Tandem Nanozymes with Elaborately Regulated Multi-Enzymatic Activities for Intensive Chemodynamic Therapy. *J. Adv. Mater.* **2022**, *34*, 2107054. [[CrossRef](#)]
66. Kainbayev, N.; Sriubas, M.; Virbukas, D.; Rutkuniene, Z.; Bockute, K.; Bolegenova, S.; Laukaitis, G. Raman study of nanocrystalline-doped ceria oxide thin films. *Coatings* **2020**, *10*, 432. [[CrossRef](#)]
67. Nayak, P.; Santhosh, P.; Ramaprabhu, S. Cerium oxide nanoparticles decorated graphene nanosheets for selective detection of dopamine. *J. Nanosci. Nanotechnol.* **2015**, *15*, 4855–4862. [[CrossRef](#)] [[PubMed](#)]
68. Durgasri, D.N.; Vinodkumar, T.; Sudarsanam, P.; Reddy, B.M. Nanosized CeO₂-Gd₂O₃ mixed oxides: Study of structural characterization and catalytic CO oxidation activity. *Catal. Lett.* **2014**, *144*, 971–979. [[CrossRef](#)]
69. Ivanov, V.K.; Shcherbakov, A.B.; Usatenko, A.V. Structure-sensitive properties and biomedical applications of nanodispersed cerium dioxide. *Russ. Chem. Rev.* **2009**, *78*, 855. [[CrossRef](#)]
70. Wang, Z.; Zeng, Y.; Li, C.; Ye, Z.; Cao, L.; Zhang, Y. Structures and electrical conductivities of Gd³⁺ and Fe³⁺ co-doped cerium oxide electrolytes sintered at low temperature for ILT-SOFCs. *Ceram. Int.* **2018**, *44*, 10328–10334. [[CrossRef](#)]
71. Chaudhary, Y.S.; Panigrahi, S.; Nayak, S.; Satpati, B.; Bhattacharjee, S.; Kulkarni, N. Facile synthesis of ultra-small monodisperse ceria nanocrystals at room temperature and their catalytic activity under visible light. *J. Mater. Chem.* **2010**, *20*, 2381–2385. [[CrossRef](#)]
72. Dunnick, K.M.; Pillai, R.; Pisane, K.L.; Stefaniak, A.B.; Sabolsky, E.M.; Leonard, S.S. The effect of cerium oxide nanoparticle valence state on reactive oxygen species and toxicity. *Biol. Trace Elem. Res.* **2015**, *166*, 96–107. [[CrossRef](#)] [[PubMed](#)]
73. Afanas'ev, I.B. Lucigenin chemiluminescence assay for superoxide detection. *Circ. Res.* **2001**, *89*, e46. [[CrossRef](#)] [[PubMed](#)]
74. Galbusera, C.; Orth, P.; Fedida, D.; Spector, T. Superoxide radical production by allopurinol and xanthine oxidase. *Biochem. Pharmacol.* **2006**, *71*, 1747–1752. [[CrossRef](#)] [[PubMed](#)]
75. Liochev, S.I.; Fridovich, I. Lucigenin as mediator of superoxide production: Revisited. *Free Radic. Biol. Med.* **1998**, *25*, 926–928. [[CrossRef](#)] [[PubMed](#)]
76. Perez, J.M.; Asati, A.; Nath, S.; Kaittanis, C. Synthesis of biocompatible dextran-coated nanoceria with pH-dependent antioxidant properties. *Small* **2008**, *4*, 552–555. [[CrossRef](#)] [[PubMed](#)]
77. Shcherbakov, A.B.; Teplonogova, M.A.; Ivanova, O.S.; Shekunova, T.O.; Ivonin, I.V.; Baranchikov, A.Y.; Ivanov, V.K. Facile method for fabrication of surfactant-free concentrated CeO₂ sols. *Mater. Res. Express* **2017**, *4*, 055008. [[CrossRef](#)]
78. Li, Y.; He, X.; Yin, J.J.; Ma, Y.; Zhang, P.; Li, J.; Ding, Y.; Zhang, J.; Zhao, Y.; Chai, Z. Acquired superoxide-scavenging ability of ceria nanoparticles. *Angew. Chem.* **2015**, *127*, 1852–1855. [[CrossRef](#)] [[PubMed](#)]
79. Khadar, Y.S.; Balamurugan, A.; Devarajan, V.; Subramanian, R. Hydrothermal synthesis of gadolinium (Gd) doped cerium oxide (CeO₂) nanoparticles: Characterization and antibacterial activity. *Orient. J. Chem.* **2017**, *33*, 2405. [[CrossRef](#)]
80. Weng, Q.; Sun, H.; Fang, C.; Xia, F.; Liao, H.; Lee, J.; Wang, J.; Xie, A.; Ren, J.; Guo, X. Catalytic activity tunable ceria nanoparticles prevent chemotherapy-induced acute kidney injury without interference with chemotherapeutics. *Nat. Commun.* **2021**, *12*, 1436. [[CrossRef](#)]
81. Soh, M.; Kang, D.W.; Jeong, H.G.; Kim, D.; Kim, D.Y.; Yang, W.; Song, C.; Baik, S.; Choi, I.Y.; Ki, S.K. Ceria-Zirconia nanoparticles as an enhanced multi-antioxidant for sepsis treatment. *Angew. Chem.* **2017**, *129*, 11557–11561. [[CrossRef](#)] [[PubMed](#)]
82. Tian, Z.; Li, X.; Ma, Y.; Chen, T.; Xu, D.; Wang, B.; Qu, Y.; Gao, Y. Quantitatively intrinsic biomimetic catalytic activity of nanoceria as radical scavengers and their ability against H₂O₂ and doxorubicin-induced oxidative stress. *ACS Appl. Mater. Interfaces* **2017**, *9*, 23342–23352. [[CrossRef](#)] [[PubMed](#)]
83. Babior, B.; Lambeth, J.; Nauseef, W. The neutrophil NADPH oxidase. *Arch. Biochem. Biophys.* **2002**, *397*, 342–344. [[CrossRef](#)] [[PubMed](#)]

84. Baranchikov, A.E.; Sozarukova, M.M.; Mikheev, I.V.; Egorova, A.A.; Proskurnina, E.V.; Poimenova, I.A.; Krasnova, S.A.; Filippova, A.D.; Ivanov, V.K. Biocompatible ligands modulate nanozyme activity of CeO₂ nanoparticles. *New J. Chem.* **2023**, *47*, 20388–20404. [[CrossRef](#)]
85. Zuo, L.; Christofi, F.L.; Wright, V.P.; Bao, S.; Clanton, T.L. Lipoxygenase-dependent superoxide release in skeletal muscle. *J. Appl. Physiol.* **2004**, *97*, 661–668. [[CrossRef](#)] [[PubMed](#)]
86. Tarnuzzer, R.W.; Colon, J.; Patil, S.; Seal, S. Vacancy engineered ceria nanostructures for protection from radiation-induced cellular damage. *Nano Lett.* **2005**, *5*, 2573–2577. [[CrossRef](#)] [[PubMed](#)]
87. Karakoti, A.S.; Singh, S.; Kumar, A.; Malinska, M.; Kuchibhatla, S.V.; Wozniak, K.; Self, W.T.; Seal, S. PEGylated nanoceria as radical scavenger with tunable redox chemistry. *J. Am. Chem. Soc.* **2009**, *131*, 14144–14145. [[CrossRef](#)]
88. Wu, H.; Li, F.; Wang, S.; Lu, J.; Li, J.; Du, Y.; Sun, X.; Chen, X.; Gao, J.; Ling, D. Ceria nanocrystals decorated mesoporous silica nanoparticle based ROS-scavenging tissue adhesive for highly efficient regenerative wound healing. *Biomaterials* **2018**, *151*, 66–77. [[CrossRef](#)]
89. Chen, B.-H.; Stephen Inbaraj, B. Various physicochemical and surface properties controlling the bioactivity of cerium oxide nanoparticles. *Crit. Rev. Biotechnol.* **2018**, *38*, 1003–1024. [[CrossRef](#)]
90. Wei, F.; Neal, C.J.; Sakthivel, T.S.; Kean, T.; Seal, S.; Coathup, M.J. Multi-functional cerium oxide nanoparticles regulate inflammation and enhance osteogenesis. *Mater. Sci. Eng. C* **2021**, *124*, 112041. [[CrossRef](#)]
91. Ghosal, M.K.; Li, X.; Beck, A.; van Bokhoven, J.A.; Artiglia, L. Size of ceria particles influences surface hydroxylation and hydroxyl stability. *J. Phys. Chem. C* **2021**, *125*, 9303–9309. [[CrossRef](#)]
92. Cafun, J.-D.; Kvashnina, K.O.; Casals, E.; Puentes, V.F.; Glatzel, P. Absence of Ce³⁺ sites in chemically active colloidal ceria nanoparticles. *ACS Nano* **2013**, *7*, 10726–10732. [[CrossRef](#)] [[PubMed](#)]
93. Yang, Y.; Mao, Z.; Huang, W.; Liu, L.; Li, J.; Li, J.; Wu, Q. Redox enzyme-mimicking activities of CeO₂ nanostructures: Intrinsic influence of exposed facets. *Sci. Rep.* **2016**, *6*, 35344. [[CrossRef](#)] [[PubMed](#)]
94. Robert, A.; Meunier, B. How to define a nanozyme. *ACS Nano* **2022**, *16*, 6956–6959. [[CrossRef](#)]
95. Zandieh, M.; Liu, J. Nanozymes: Definition, activity, and mechanisms. *Adv. Mater.* **2023**, *36*, 2211041. [[CrossRef](#)] [[PubMed](#)]
96. Vladimirov, G.; Sergunova, E.; Izmaylov, D.; Vladimirov, Y. Chemiluminescent determination of total antioxidant capacity in medicinal plant material. *Bull. Russ. State Med. Univ.* **2016**, *2016*, 62–68. [[CrossRef](#)]
97. Garcia-Salvador, A.; Katsumi, A.; Rojas, E.; Aristimuno, C.; Betanzos, M.; Martinez-Moro, M.; Moya, S.E.; Goni-de-Cerio, F. A Complete In Vitro Toxicological Assessment of the Biological Effects of Cerium Oxide Nanoparticles: From Acute Toxicity to Multi-Dose Subchronic Cytotoxicity Study. *Nanomaterials* **2021**, *11*, 1577. [[CrossRef](#)] [[PubMed](#)]
98. Inbaraj, B.S.; Chen, B.-H. An overview on recent in vivo biological application of cerium oxide nanoparticles. *Asian J. Pharm. Sci.* **2020**, *15*, 558–575. [[CrossRef](#)]
99. Datta, A.; Mishra, S.; Manna, K.; Saha, K.D.; Mukherjee, S.; Roy, S. Pro-oxidant therapeutic activities of cerium oxide nanoparticles in colorectal carcinoma cells. *ACS Omega* **2020**, *5*, 9714–9723. [[CrossRef](#)]

Disclaimer/Publisher's Note: The statements, opinions and data contained in all publications are solely those of the individual author(s) and contributor(s) and not of MDPI and/or the editor(s). MDPI and/or the editor(s) disclaim responsibility for any injury to people or property resulting from any ideas, methods, instructions or products referred to in the content.